CHAPTER 8

NUMERICAL SOLUTION OF A TWO-DIMENSIONAL SUPERSONIC FLOW: PRANDTL-MEYER EXPANSION WAVE

The error therefore lyeth neither in the abstract nor in geometry, nor in physicks, but in the calculator, that knoweth not how to adjust his accompts.

Galileo Galilei, 1632

8.1 INTRODUCTION

In the above quote, Galileo was expressing a concern with the role of mathematics in the analysis of real physical problems. Prior to the seventeenth century, driven by the concepts of Aristotelian physics, the prevailing method was to accept geometric purity as the explanation for much physical phenomena. The concepts of the physical world were bent and adjusted so as to be in harmony with perfect geometry. For example, a perfect sphere touches a plane at only one point, whereas a real ball (such as a basketball) touches the floor over a finite surface area—the basketball has a small finite flat region in contact with the floor; hence it is not a perfect sphere. Early mathematicians would have assumed the basketball to be a perfect sphere

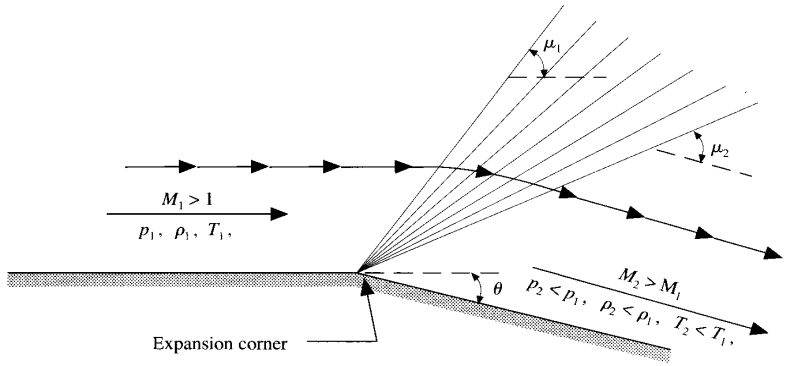

FIG. 8.1
Centered Prandtl-Meyer expansion wave.

touching the floor at only one point; they would not have considered an analysis of a ball with a flat spot to be of any value in mathematics, or in nature. In the early seventeenth century, Galileo was reacting to this altitude. In his *Dialogue Concerning the Two Chief Systems of the World, the Ptolemaic and the Copernican*, from which the above quote is taken, Galileo argued that the role of mathematics is to adjust to the real physical world, and not vice versa. The mathematics for studying the basketball should be adjusted to *account* for the flat spot, not rule it away. The person making the calculation (the "calculator" in the above quote) must know how to adjust his or her mathematical analysis (the "accompts" in the above quote) to match the physics. Little did Galileo realize that he was estabilishing a basic tenet of CFD, namely, the effort to adjust numerical mathematics to the real physical problem. We will see a graphic example of such a philosophy in the present chapter.

The type of flow highlighted in the present chapter is a two-dimensional, inviscid, supersonic flow moving over a surface. In this type of problem, it is particularly vital to couple the surface boundary condition into the flow-field calculation—to make certain that the inviscid flow readily sees the shape of the surface over which it is flowing. Here we will be seriously concerned with how to "adjust" the numerical mathematics to properly "see" the shape of the boundary.

The discussion in the present chapter is an illustration of the *downstream marching* (*or space marching*) philosophy described in Sec. 6.4.3. This is in contrast to the time-marching technique illustrated in Chap. 7. Downstream marching is used in many standard CFD codes today, so this chapter has much relevance. Make certain to review Sec. 6.4.3 before proceeding further. MacCormack's space marching technique as described in Sec. 6.4.3 will be applied for the solution of the two-dimensional supersonic flow problem highlighted in the present chapter.

Specifically, we choose to numerically solve the inviscid flow over an expansion corner, as sketched in Fig. 8.1. This problem is in keeping with our

philosophy of choosing flow problems for which an exact analytical solution exists in order to obtain a reasonable feeling for the accuracy of the numerical technique.

Finally, the road map for this chapter is given as Fig. 8.9, near the end of the chapter. Make certain to examine this road map as you progress through the various sections. In addition, reexamine Fig. 1.32*e*, which illustrates the flow of various ideas that impact this application.

8.2 INTRODUCTION TO THE PHYSICAL PROBLEM: PRANDTL–MEYER EXPANSION WAVE—EXACT ANALYTIC SOLUTION

A centered, Prandtl–Meyer expansion wave is illustrated in Fig. 8.1. Here, a supersonic flow is expanded around a sharp expansion corner. An expansion wave, made up of an infinite number of infinitely weak Mach waves, fans out from the corner, as shown in Fig. 8.1. The leading edge of the expansion fan makes an angle μ_1 with respect to the upstream flow direction, and the trailing edge of the wave makes an angle μ_2 with respect to the downstream flow direction. The angles μ_1 and μ_2 are Mach angles, defined by

$$\mu_1 = \sin^{-1}\frac{1}{M_1} \qquad \text{and} \qquad \mu_2 = \sin^{-1}\frac{1}{M_2}$$

where M_1 and M_2 are the upstream and downstream Mach numbers, respectively. The flow through an expansion wave is isentropic. As the flow passes through the expansion wave, the Mach number increases and the pressure, temperature, and density decrease; these trends are noted in Fig. 8.1. The flow in front of the centered expansion wave is uniform at a Mach number M_1 and is parallel to the wall in front of the wave. The flow behind the expansion wave is also uniform at a Mach number of M_2 and is parallel to the wall behind the wave. Inside the wave itself, the flow properties change smoothly, and the streamlines are curved, as sketched in Fig. 8.1. Inside the wave, the flow is two-dimensional. The only exception to the above discussion is right at the corner itself; this is a singular point at which the streamline at the wall experiences a discontinuous change in direction and where the flow properties are discontinuous. This singularity has some impact on the numerical solution of the flow field, as you might suspect. Such matters will be addressed in a subsequent section. For given supersonic upstream conditions and a given flow deflection angle θ at the corner, the downstream conditions (denoted by a subscript 2) are uniquely defined. For a calorically perfect gas, there is an exact, analytical solution for the conditions behind the expansion wave, as outlined below. Many more details associated with a Prandtl–Meyer expansion can be found in Refs. 8 and 21.

The analytical solution of the flow across a centered expansion wave hinges on the simple relation

$$f_2 = f_1 + \theta \tag{8.1}$$

where f is the Prandtl–Meyer function and θ is the flow deflection angle shown in Fig. 8.1. For a calorically perfect gas, the Prandtl–Meyer function depends on M and γ and is given by

$$f = \sqrt{\frac{\gamma+1}{\gamma-1}}\tan^{-1}\sqrt{\frac{\gamma-1}{\gamma+1}(M^2-1)} - \tan^{-1}\sqrt{M^2-1} \tag{8.2}$$

The analytical solution proceeds as follows. For the given M_1, calculate f_1 from Eq. (8.2). Then, for the given θ, calculate f_2 from Eq. (8.1). The Mach number in region 2 is then obtained by solving (implicitly, by trial and error) Eq. (8.2) for M_2, using the value of f_2 obtained above. Once M_2 is obtained, then the pressure, temperature, and density behind the wave are calculated from the isentropic flow relations

$$p_2 = p_1\left\{\frac{1+[(\gamma-1)/2]M_1^2}{1+[(\gamma-1)/2]M_2^2}\right\}^{\gamma/(\gamma-1)} \tag{8.3}$$

$$T_2 = T_1\frac{1+[(\gamma-1)/2]M_1^2}{1+[(\gamma-1)/2]M_2^2} \tag{8.4}$$

and the equation of state

$$\rho_2 = \frac{p_2}{RT_2} \tag{8.5}$$

With Eqs. (8.1) to (8.5), the flow behind the centered expansion wave is completely determined.

8.3 THE NUMERICAL SOLUTION OF A PRANDTL–MEYER EXPANSION WAVE FLOW FIELD

In this chapter we will carry out a downstream marching solution for the supersonic flow over an expansion corner. The solution technique will be MacCormack's predictor-corrector explicit finite-difference method. The details of this downstream (or space) marching approach are given in Sec. 6.4.3. Make certain that you feel comfortable with the contents of Sec. 6.4.3 before progressing further.

8.3.1 The Governing Equations

The governing Euler equations for a steady, two-dimensional flow in strong conservation form can be expressed in the generic form given by Eq. (6.24), repeated below:

$$\frac{\partial F}{\partial x} = J - \frac{\partial G}{\partial y} \tag{6.24}$$

where F and G are column vectors with elements defined by Eqs. (2.106) and (2.107), respectively, repeated below.

$$F = \begin{Bmatrix} \rho u \\ \rho u^2 + p \\ \rho uv \\ \rho u\left(e + \frac{V^2}{2}\right) + pu \end{Bmatrix} \tag{2.106}$$

$$G = \begin{Bmatrix} \rho v \\ \rho uv \\ \rho v^2 + p \\ \rho v\left(e + \frac{V^2}{2}\right) + pv \end{Bmatrix} \tag{2.107}$$

We are considering isentropic (hence adiabatic) flow with no body forces; therefore, the source term denoted by J in Eq. (6.24) is, from Eq. (2.109), equal to zero. For clarity in our subsequent calculations, we will denote each of the elements in the column vector expressed by Eq. (2.106) as follows:

$$F_1 = \rho u \tag{8.6a}$$

$$F_2 = \rho u^2 + p \tag{8.6b}$$

$$F_3 = \rho uv \tag{8.6c}$$

$$F_4 = \rho u\left(e + \frac{u^2 + v^2}{2}\right) + pu \tag{8.6d}$$

For a calorically perfect gas, it is convenient to eliminate e in Eq. (8.6*d*) in favor of p and ρ as follows.

$$e = c_v T = \frac{RT}{\gamma - 1} = \frac{1}{\gamma - 1}\frac{p}{\rho}$$

Hence, Eq. (8.6*d*) can be written as

$$F_4 = \rho u\left(\frac{1}{\gamma - 1}\frac{p}{\rho} + \frac{u^2 + v^2}{2}\right) + pu$$

$$= \frac{1}{\gamma - 1} pu + \rho u \frac{u^2 + v^2}{2} + pu$$

Combining the terms involving pu, we have

$$F_4 = \frac{\gamma}{\gamma - 1} pu + \rho u \frac{u^2 + v^2}{2} \tag{8.6e}$$

Also, the elements of the column vector expressed by Eq. (2.107) are denoted by

$$G_1 = \rho v \tag{8.7a}$$

$$G_2 = \rho uv \tag{8.7b}$$

$$G_3 = \rho v^2 + p \tag{8.7c}$$

$$G_4 = \rho v\left(e + \frac{u^2 + v^2}{2}\right) + pv \tag{8.7d}$$

In a fashion analogous to that carried out for Eq. (8.6*e*), we can express Eq. (8.7*d*) as

$$G_4 = \frac{\gamma}{\gamma - 1} pv + \rho v \frac{u^2 + v^2}{2} \tag{8.7e}$$

The essence of the downstream marching solution, to be discussed shortly, can be presaged by examining the above equations. Note that Eq. (6.24) is written with the x derivative on the left-hand side and the y derivative on the right-hand side. Examining Fig. 8.2, if the flow-field variables are given at location x_0 as a function of y along an *initial data line* (the dashed line in Fig. 8.2), then the y derivative of G in Eq. (6.24) is known along this line. This allows the x derivative of F to be calculated. With this known x derivative, we can advance the flow-field variables to the next vertical line located at $x_0 + \Delta x$. In this fashion, the solution can be carried out by marching in steps of Δx along the x direction in Fig. 8.2, starting with the specified flow field along the initial data line.

We recall from our discussion in Sec. 6.4.3 that, for a downstream marching solution, we *have* to employ the governing equations in the strong conservation form given by Eq. (6.24); this is the only form in which a *single* x derivative can be couched on the left-hand side of the equation. Therefore, as you might suspect from our experience with the strong conservation form of the equations in Chap. 7, there

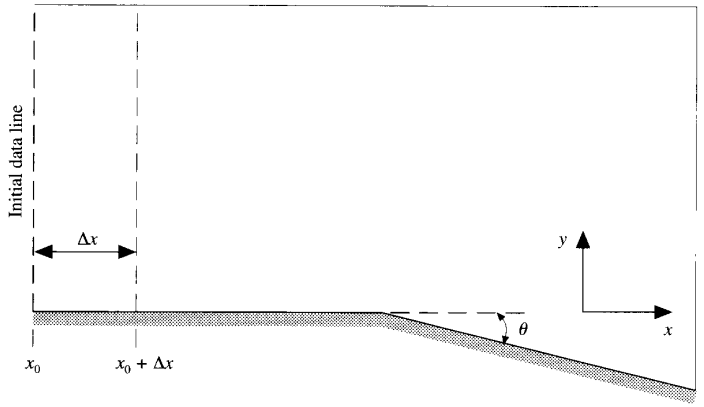

FIG. 8.2
Model for the downstream marching solution.

is some extra baggage that goes along with the numerical solution of this form of the equations, namely, (1) the need to *decode* the primitive variables from the flux variables F_1, F_2, F_3, and F_4, and (2) the corresponding desirability of expressing the elements of the G vector, G_1, G_2, G_3, and G_4, in a "pure" form involving F_1, F_2, F_3, and F_4 rather than the primitive variables as originally defined in Eqs. (8.7*a*) to (8.7*e*). Let us proceed with a discussion of these two items.

For decoding the primitive variables from the flux variables, we will simply write down the results because the derivation is assigned as Prob. 2.1; i.e., the answer to Prob. 2.1 is as follows:

$$\rho = \frac{-B + \sqrt{B^2 - 4AC}}{2A} \tag{8.8}$$

where

$$A = \frac{F_3^2}{2F_1} - F_4$$

$$B = \frac{\gamma}{\gamma - 1} F_1 F_2$$

$$C = -\frac{\gamma + 1}{2(\gamma - 1)} F_1^3$$

$$u = \frac{F_1}{\rho} \tag{8.9}$$

$$v = \frac{F_3}{F_1} \tag{8.10}$$

$$p = F_2 - F_1 u \tag{8.11}$$

and from the equation of state

$$T = \frac{p}{\rho R} \tag{8.12}$$

Note that the solution for ρ involves a quadratic equation. Because of this, the decoding for the primitive variables for the present case of the *steady* flow equations in the form of Eq. (6.24) requires a more rigorous derivation than the rather straightforward decoding when the *unsteady* flow equations are used in the form of Eq. (2.99), where the decoding is given by Eqs. (2.100) to (2.104). We took advantage of this more straightforward decoding in Chap. 7 where in part we dealt with the unsteady equations in the form of Eqs. (7.101*a*) to (7.101*c*), with the decoding given by Eqs. (7.102) to (7.105).

As we have noted before, when the strong conservation form of the governing equations is used for a numerical solution, specifically when Eq. (6.24) is used, numbers are directly obtained for the fluxes F_1, F_2, F_3, and F_4—*not* the primitive variables. The corresponding values of ρ, u, v, p, and T have to be obtained after the fact from Eqs. (8.8) to (8.12).

We now address a related matter, namely, the way in which the values of G in Eq. (6.24) are calculated. Since values of F_1, F_2, F_3, and F_4 are directly calculated

at a given grid point from our numerical solution of Eq. (6.24), it makes sense to return these numbers back to the equation in the form of G_1, G_2, G_3, and G_4 for the calculation at the next downstream-located grid point. That is, it makes sense to calculate numbers for G_1, G_2, G_3, and G_4 *directly* from the numbers obtained for F_1, F_2, F_3, and F_4, rather than going through the intermediate step of extracting the primitive variables by using Eqs. (8.8) to (8.12) and then synthesizing G_1, G_2, G_3, and G_4 from these primitive variables as given in the definitions of the G's in Eqs. (8.7*a*) to (8.7*e*). Indeed, the G's are clearly functions of the F's; let us obtain these functions.

To begin with, from Eqs. (8.7*a*) and (8.10), we have

$$G_1 = \rho v = \rho \frac{F_3}{F_1} \tag{8.13}$$

In Eq. (8.13), ρ can be expressed in terms of F_1, F_2, F_3, and F_4 via Eq. (8.8); since this is a quadratic relationship, we will not bother to substitute the complicated expression into Eq. (8.13). From Eqs. (8.6*c*) and (8.7*b*), we can write directly for G_2,

$$G_2 = F_3 \tag{8.14}$$

From Eqs. (8.7*c*) and (8.10), we can write

$$G_3 = \rho v^2 + p = \rho \left(\frac{F_3}{F_1}\right)^2 + p \tag{8.15}$$

We can eliminate p from Eq. (8.15) by combining Eqs. (8.6*b*) and (8.9) as follows:

$$p = F_2 - \rho u^2 = F_2 - \frac{F_1^2}{\rho} \tag{8.16}$$

Substituting Eq. (8.16) into (8.15), we have

$$G_3 = \rho \left(\frac{F_3}{F_1}\right)^2 + F_2 - \frac{F_1^2}{\rho} \tag{8.17}$$

Finally, an expression for G_4 can be constructed as follows. From Eqs. (8.7*e*), (8.10), and (8.16), we have

$$\begin{aligned} G_4 &= \frac{\gamma}{\gamma - 1} pv + \rho v \frac{u^2 + v^2}{2} \\ &= \frac{\gamma}{\gamma - 1} \left(F_2 - \frac{F_1^2}{\rho}\right) \frac{F_3}{F_1} + \frac{\rho}{2} \frac{F_3}{F_1} \left[\left(\frac{F_1}{\rho}\right)^2 + \left(\frac{F_3}{F_1}\right)^2 \right] \end{aligned} \tag{8.18}$$

In summary, Eqs. (8.13), (8.14), (8.17), and (8.18) give expressions for G_1, G_2, G_3, and G_4 as functions of F_1, F_2, F_3, and F_4 [keeping in mind that ρ in these equations is itself a function of F_1, F_2, F_3, and F_4 via Eq. (8.8)]. When the values of G_1, G_2, G_3, and G_4 are calculated from these equations [rather than from the primitive variables by using Eqs. (8.7*a*) to (8.7*e*)], then we are using a "purer" formulation of the strong conservation form of the governing equations, in the same spirit as discussed in Sec. 7.5.2.

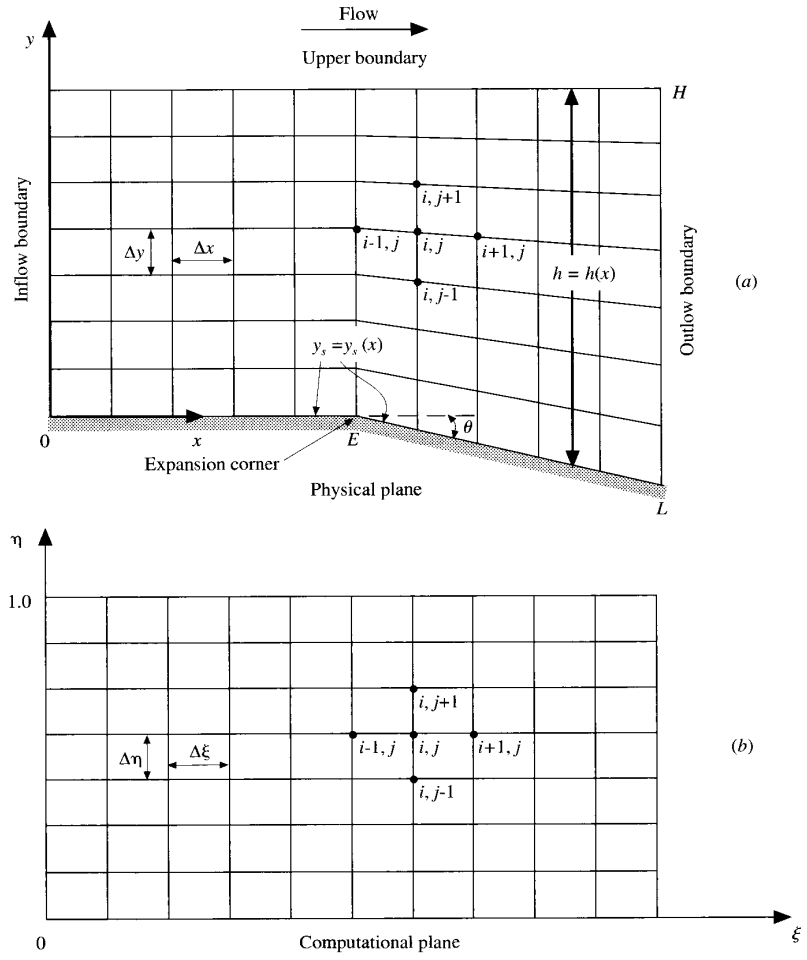

FIG. 8.3
The (*a*) physical and (*b*) computational planes for the numerical solution of the centered expansion wave problem.

THE TRANSFORMATION. The present problem affords us an opportunity to exercise some of the aspects of grid generation and equation transformation that were discussed in Chap. 5. In particular, to set up a finite-difference solution for the flow over an expansion corner, we must use a boundary-fitted coordinate system, as sketched in Fig. 8.3. The physical plane using an xy cartesian coordinate system is shown in Fig. 8.3*a*. The surface including the expansion corner forms the lower

boundary in this physical space. The inflow boundary occurs at $x = 0$, and the outflow boundary is at $x = L$. The upper boundary is chosen as a horizontal line at a rather arbitrary value of $y = H$. Clearly, the physical space, due to the downward-sloping wall downstream of the expansion corner, does not lend itself to a completely rectangular grid. Therefore, we must transform the physical plane to a computational plane where the finite-difference grid *is* rectangular, as shown in Fig. 8.3*b*. The computational plane is couched in terms of ξ and η as the independent variables. The bottom surface in the physical plane should correspond to a constant η coordinate curve; i.e., we need to establish a *boundary-fitted coordinate system*. Boundary-fitted coordinate systems are discussed in some detail in Sec. 5.7. In the present application, we need only a *simple* boundary-fitted coordinate system, much along the lines given by Eqs. (5.65) and (5.66). Before continuing further, return to Sec. 5.7 and review the first part having to do with a simple boundary-fitted, algebraically generated grid.

Examining Fig. 8.3*a*, we can readily construct a proper transformation as follows. Let h denote the local height from the lower to the upper boundary in the physical plane; clearly, $h = h(x)$. Denote the y location of the solid surface (the lower boundary in the physical plane) by y_s, where $y_s = y_s(x)$. With this, we define the transformation as

$$\xi = x \tag{8.19}$$

$$\eta = \frac{y - y_s(x)}{h(x)} \tag{8.20}$$

With this transformation, in the computational plane ξ varies from 0 to L and η varies from 0 to 1.0; $\eta = 0$ corresponds to the surface in the physical plane, and $\eta = 1.0$ corresponds to the upper boundary. The lines of constant ξ and η form a regular rectangular grid in the computational plane (Fig. 8.3*b*). The lines of constant ξ and η are also sketched in the physical plane (Fig. 8.3*a*); they form a rectangular grid upstream of the corner and a network of divergent lines downstream of the corner.

As discussed in Chap. 5, we carry out the finite-difference calculations on the rectangular grid in the $\xi\eta$ plane. The partial differential equations for the flow are numerically solved in the transformed space and therefore must be appropriately transformed for use in the transformed, computational plane. That is, Eq. (6.24) must be transformed into terms dealing with ξ and η. The derivative transformation is given by Eqs. (5.2) and (5.3), repeated below.

$$\frac{\partial}{\partial x} = \frac{\partial}{\partial \xi}\left(\frac{\partial \xi}{\partial x}\right) + \frac{\partial}{\partial \eta}\left(\frac{\partial \eta}{\partial x}\right) \tag{5.2}$$

$$\frac{\partial}{\partial y} = \frac{\partial}{\partial \xi}\left(\frac{\partial \xi}{\partial y}\right) + \frac{\partial}{\partial \eta}\left(\frac{\partial \eta}{\partial y}\right) \tag{5.3}$$

The metrics in Eqs. (5.2) and (5.3) are obtained from the transformation given by Eqs. (8.19) and (8.20), that is,

$$\frac{\partial \xi}{\partial x} = 1 \tag{8.21}$$

$$\frac{\partial \xi}{\partial y} = 0 \tag{8.22}$$

$$\frac{\partial \eta}{\partial x} = -\frac{1}{h}\frac{dy_s}{dx} - \frac{\eta}{h}\frac{dh}{dx} \tag{8.23}$$

$$\frac{\partial \eta}{\partial y} = \frac{1}{h} \tag{8.24}$$

The metric $\partial\eta/\partial x$ in Eq. (8.23) can be expressed in a simpler way, as follows. Examining Fig. 8.3*a*, and denoting the x location of the expansion corner by $x = E$, we have

For $x \leq E$:

$$y_s = 0$$
$$h = \text{constant}$$

For $x \geq E$:

$$y_s = -(x - E)\tan\theta$$
$$h = H + (x - E)\tan\theta$$

Differentiating these expressions, we have

For $x \leq E$:

$$\frac{dy_s}{dx} = 0$$
$$\frac{dh}{dx} = 0$$

For $x \geq E$:

$$\frac{dy_s}{dx} = -\tan\theta$$
$$\frac{dh}{dx} = \tan\theta$$

Hence, the metric $\partial\eta/\partial x$ can be written as

$$\frac{\partial \eta}{\partial x} = \begin{cases} 0 & \text{for } x \leq E \quad (8.25a) \\ (1 - \eta)\dfrac{\tan\theta}{h} & \text{for } x \geq E \quad (8.25b) \end{cases}$$

The complete derivative transformation is obtained by substituting Eqs. (8.21), (8.22), (8.24), and (8.25) into (5.2) and (5.3), obtaining

$$\boxed{\frac{\partial}{\partial x} = \frac{\partial}{\partial \xi} + \left(\frac{\partial \eta}{\partial x}\right)\frac{\partial}{\partial \eta}} \tag{8.26}$$

and

$$\boxed{\frac{\partial}{\partial y} = \frac{1}{h}\frac{\partial}{\partial \eta}} \tag{8.27}$$

where in Eq. (8.26), $\partial\eta/\partial x$ is given by either one of Eqs. (8.25*a*) or (8.25*b*), as appropriate.

Return to the governing flow equations in conservation form, given in the physical plane by Eq. (6.24). With $J = 0$, this equation becomes

$$\frac{\partial F}{\partial x} = -\frac{\partial G}{\partial y} \tag{8.28}$$

Transforming Eq. (8.28) via Eqs. (8.26) and (8.27), we have

$$\frac{\partial F}{\partial \xi} + \left(\frac{\partial \eta}{\partial x}\right)\frac{\partial F}{\partial \eta} = -\frac{1}{h}\frac{\partial G}{\partial n}$$

or

$$\boxed{\frac{\partial F}{\partial \xi} = -\left[\left(\frac{\partial \eta}{\partial x}\right)\frac{\partial F}{\partial \eta} + \frac{1}{h}\frac{\partial G}{\partial \eta}\right]} \tag{8.29}$$

where the metric term $\partial\eta/\partial x$ is given by Eq. (8.25*a*) or (8.25*b*), as appropriate. Written in terms of the elements of the column vectors F and G, Eq. (8.29) represents the following system of equations, where the labels are added to remind you of the physical origin of each equation.

$$\boxed{\begin{aligned} &\textit{Continuity}: && \frac{\partial F_1}{\partial \xi} = -\left[\left(\frac{\partial \eta}{\partial x}\right)\frac{\partial F_1}{\partial \eta} + \frac{1}{h}\frac{\partial G_1}{\partial \eta}\right] && (8.30) \\ &x\ \textit{momentum}: && \frac{\partial F_2}{\partial \xi} = -\left[\left(\frac{\partial \eta}{\partial x}\right)\frac{\partial F_2}{\partial \eta} + \frac{1}{h}\frac{\partial G_2}{\partial \eta}\right] && (8.31) \\ &y\ \textit{momentum}: && \frac{\partial F_3}{\partial \xi} = -\left[\left(\frac{\partial \eta}{\partial x}\right)\frac{\partial F_3}{\partial \eta} + \frac{1}{h}\frac{\partial G_3}{\partial \eta}\right] && (8.32) \\ &\textit{Energy}: && \frac{\partial F_4}{\partial \xi} = -\left[\left(\frac{\partial \eta}{\partial x}\right)\frac{\partial F_4}{\partial \eta} + \frac{1}{h}\frac{\partial G_4}{\partial \eta}\right] && (8.33) \end{aligned}}$$

Equations (8.30) to (8.33) are the governing flow equations which are to be solved numerically in the computational plane sketched in Fig. 8.3*b*.

Note: Equations (8.30) to (8.33) are in *dimensional* form; we have not bothered to nondimensionalize the variables in the equations, in contrast to the approach taken in Chap. 7. Indeed, in the present solution, we will continue to treat all variables in their dimensional form—just to illustrate that a CFD solution can just as well be carried out using numbers with units attached to them and that the use of dimensionless variables is in no way necessary for the integrity of a CFD

solution. In fact, an advantage of using dimensional variables in a numerical solution is that you quickly obtain an engineering feeling for the magnitudes of the physical properties in a given flow problem. The choice of using nondimensional variables is simply up to you; for some problems it makes more sense than others—for example, the convenience of dealing with nondimensional variables for the quasi-one-dimensional flow problem was amply demonstrated in Chap. 7. However, when you use *dimensional* variables, it is vitally important that you *keep the units straight*. For this reason, it is strongly recommended that you use a *consistent set of units* throughout your calculation. The equations discussed in this section hold in their precise form as long as consistent units are employed; i.e., there is no need to insert any "conversion factor" in the equations as would be the case when inconsistent units are employed. See, for example, Chap. 2 of Ref. 1 for a discussion of what is meant by consistent and inconsistent units. Two common sets of consistent units are the English engineering system (pound, slug, foot, second, degree Rankine) and the international, SI system (newton, kilogram, meter, second, kelvin). In this present solution, we will use SI units. Again, keep in mind that when you choose to use dimensional properties in your CFD calculation, you incur the necessity to handle the units correctly.

This finishes our development of the general equations germane to the given problem. Let us now proceed with the solution.

8.3.2 The Setup

We need to establish some details of the particular problem to be solved. We consider the detailed physical plane drawn to scale in Fig. 8.4. The flow at the

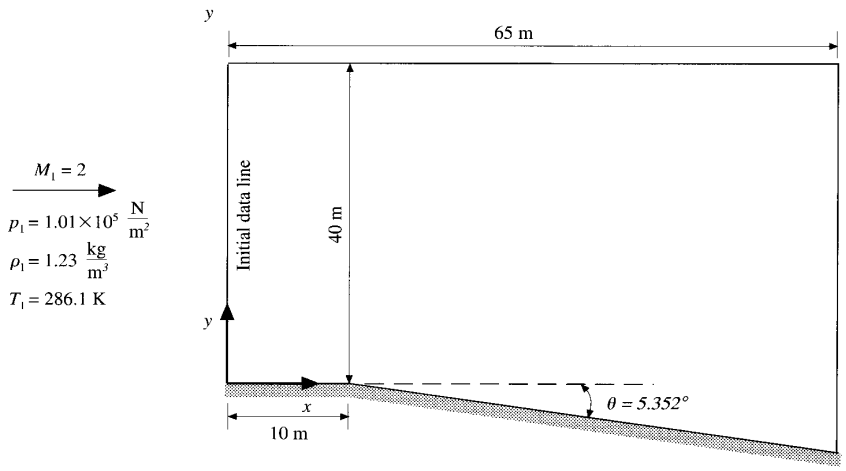

FIG. 8.4
Physical plane, drawn to scale.

upstream boundary is at Mach 2 with a pressure, density, and temperature equal to 1.01×10^5 N/m^2, 1.23 kg/m^3, and 286 K, respectively. The supersonic flow is expanded through an angle of 5.352°, as shown in Fig. 8.4. This is a rather mild expansion angle; the reasons for this choice will be discussed later. The calculations will be made in the domain from $x = 0$ to $x = 65$ m and from the wall to $y = 40$ m, as shown in Fig. 8.4. The location of the expansion corner is at $x = 10$ m. For this geometry, the variation of $h = h(x)$ is given by

$$h = \begin{cases} 40 \text{ m} & 0 \le x \le 10 \text{ m} \quad (8.34) \\ 40 + (x - 10)\tan\theta & 10 \le x \le 65 \text{ m} \quad (8.35) \end{cases}$$

Equation (8.34) or (8.35), as appropriate, is needed to define the value of the metric $\partial\eta/\partial x$ expressed by Eq. (8.25*b*).

INITIAL DATA LINE. The initial data line is given by $x = 0$; along this vertical line at each grid point, the initial data are fed in, equal to the uniform upstream flow conditions. The calculation starts at this initial data line and marches downstream in steps of Δx. For our application, we will divide the $x = 0$ initial data line into 40 increments by evenly spacing 41 grid points ($j = 1$ to 41) along this line. To reinforce this picture, the initial data at $x = 0$ is tabulated in Table 8.1 versus j.

FINITE-DIFFERENCE EQUATIONS. We are following the technique set forth in Sec. 6.4.3, which outlines MacCormack's predictor-corrector technique applied to space marching (note that space marching and downstream marching are synonymous terms). Hence, the finite-difference forms of Eq. (8.30) to (8.33) are as follows.

Predictor step. Analogous to Eq. (6.26), Eqs. (8.30) to (8.33) are written in terms of forward differences.

$$\left(\frac{\partial F_1}{\partial \xi}\right)_{i,j} = \left(\frac{\partial \eta}{\partial x}\right)\frac{(F_1)_{i,j} - (F_1)_{i,j+1}}{\Delta\eta} + \frac{1}{h}\frac{(G_1)_{i,j} - (G_1)_{i,j+1}}{\Delta\eta} \quad (8.36a)$$

$$\left(\frac{\partial F_2}{\partial \xi}\right)_{i,j} = \left(\frac{\partial \eta}{\partial x}\right)\frac{(F_2)_{i,j} - (F_2)_{i,j+1}}{\Delta\eta} + \frac{1}{h}\frac{(G_2)_{i,j} - (G_2)_{i,j+1}}{\Delta\eta} \quad (8.36b)$$

$$\left(\frac{\partial F_3}{\partial \xi}\right)_{i,j} = \left(\frac{\partial \eta}{\partial x}\right)\frac{(F_3)_{i,j} - (F_3)_{i,j+1}}{\Delta\eta} + \frac{1}{h}\frac{(G_3)_{i,j} - (G_3)_{i,j+1}}{\Delta\eta} \quad (8.36c)$$

$$\left(\frac{\partial F_4}{\partial \xi}\right)_{i,j} = \left(\frac{\partial \eta}{\partial x}\right)\frac{(F_4)_{i,j} - (F_4)_{i,j+1}}{\Delta\eta} + \frac{1}{h}\frac{(G_4)_{i,j} - (G_4)_{i,j+1}}{\Delta\eta} \quad (8.36d)$$

TABLE 8.1
Initial conditions at $x = 0$

j	u, m/s	v, m/s	ρ, kg/m^3	p, N/m^2	T, K	M
1	.678E+03	.000E+00	.123E+01	.101E+06	.286E+03	.200E+01
2	.678E+03	.000E+00	.123E+01	.101E+06	.286E+03	.200E+01
3	.678E+03	.000E+00	.123E+01	.101E+06	.286E+03	.200E+01
4	.678E+03	.000E+00	.123E+01	.101E+06	.286E+03	.200E+01
5	.678E+03	.000E+00	.123E+01	.101E+06	.286E+03	.200E+01
6	.678E+03	.000E+00	.123E+01	.101E+06	.286E+03	.200E+01
7	.678E+03	.000E+00	.123E+01	.101E+06	.286E+03	.200E+01
8	.678E+03	.000E+00	.123E+01	.101E+06	.286E+03	.200E+01
9	.678E+03	.000E+00	.123E+01	.101E+06	.286E+03	.200E+01
10	.678E+03	.000E+00	.123E+01	.101E+06	.286E+03	.200E+01
11	.678E+03	.000E+00	.123E+01	.101E+06	.286E+03	.200E+01
12	.678E+03	.000E+00	.123E+01	.101E+06	.286E+03	.200E+01
13	.678E+03	.000E+00	.123E+01	.101E+06	.286E+03	.200E+01
14	.678E+03	.000E+00	.123E+01	.101E+06	.286E+03	.200E+01
15	.678E+03	.000E+00	.123E+01	.101E+06	.286E+03	.200E+01
16	.678E+03	.000E+00	.123E+01	.101E+06	.286E+03	.200E+01
17	.678E+03	.000E+00	.123E+01	.101E+06	.286E+03	.200E+01
18	.678E+03	.000E+00	.123E+01	.101E+06	.286E+03	.200E+01
19	.678E+03	.000E+00	.123E+01	.101E+06	.286E+03	.200E+01
20	.678E+03	.000E+00	.123E+01	.101E+06	.286E+03	.200E+01
21	.678E+03	.000E+00	.123E+01	.101E+06	.286E+03	.200E+01
22	.678E+03	.000E+00	.123E+01	.101E+06	.286E+03	.200E+01
23	.678E+03	.000E+00	.123E+01	.101E+06	.286E+03	.200E+01
24	.678E+03	.000E+00	.123E+01	.101E+06	.286E+03	.200E+01
25	.678E+03	.000E+00	.123E+01	.101E+06	.286E+03	.200E+01
26	.678E+03	.000E+00	.123E+01	.101E+06	.286E+03	.200E+01
27	.678E+03	.000E+00	.123E+01	.101E+06	.286E+03	.200E+01
28	.678E+03	.000E+00	.123E+01	.101E+06	.286E+03	.200E+01
29	.678E+03	.000E+00	.123E+01	.101E+06	.286E+03	.200E+01
30	.678E+03	.000E+00	.123E+01	.101E+06	.286E+03	.200E+01
31	.678E+03	.000E+00	.123E+01	.101E+06	.286E+03	.200E+01
32	.678E+03	.000E+00	.123E+01	.101E+06	.286E+03	.200E+01
33	.678E+03	.000E+00	.123E+01	.101E+06	.286E+03	.200E+01
34	.678E+03	.000E+00	.123E+01	.101E+06	.286E+03	.200E+01
35	.678E+03	.000E+00	.123E+01	.101E+06	.286E+03	.200E+01
36	.678E+03	.000E+00	.123E+01	.101E+06	.286E+03	.200E+01
37	.678E+03	.000E+00	.123E+01	.101E+06	.286E+03	.200E+01
38	.678E+03	.000E+00	.123E+01	.101E+06	.286E+03	.200E+01
39	.678E+03	.000E+00	.123E+01	.101E+06	.286E+03	.200E+01
40	.678E+03	.000E+00	.123E+01	.101E+06	.286E+03	.200E+01
41	.678E+03	.000E+00	.123E+01	.101E+06	.286E+03	.200E+01

The predicted values of F are obtained as follows, analogous to Eq. (6.27).

$$(\bar{F}_1)_{i+1,j} = (F_1)_{i,j} + \left(\frac{\partial F_1}{\partial \xi}\right)_{i,j} \Delta\xi \tag{8.37a}$$

$$(\bar{F}_2)_{i+1,j} = (F_2)_{i,j} + \left(\frac{\partial F_2}{\partial \xi}\right)_{i,j} \Delta\xi \tag{8.37b}$$

$$(\bar{F}_3)_{i+1,j} = (F_3)_{i,j} + \left(\frac{\partial F_3}{\partial \xi}\right)_{i,j} \Delta\xi \tag{8.37c}$$

$$(\bar{F}_4)_{i+1,j} = (F_4)_{i,j} + \left(\frac{\partial F_4}{\partial \xi}\right)_{i,j} \Delta\xi \tag{8.37d}$$

Before proceeding to the corrector step, we need to decode the values of $\bar{F}_{i+1,j}$. This is carried out using Eq. (8.8).

$$(\bar{\rho})_{i+1,j} = \frac{-B + \sqrt{B^2 - 4AC}}{2A} \tag{8.38}$$

where

$$A = \frac{(\bar{F}_3)^2_{i+1,j}}{2(\bar{F}_1)_{i+1,j}} - (\bar{F}_4)_{i+1,j}$$

$$B = \frac{\gamma}{\gamma - 1}(\bar{F}_1)_{i+1,j}(\bar{F}_2)_{i+1,j}$$

$$C = -\frac{\gamma + 1}{2(\gamma - 1)}(\bar{F}_1)^3_{i+1,j}$$

With the predicted values of ρ obtained above, we can form the predicted values of G, which are needed for the corrector step. From Eqs. (8.13), (8.14), (8.17), and (8.18), we have, respectively,

$$(\bar{G}_1)_{i+1,j} = \bar{\rho}_{i+1,j}\frac{(\bar{F}_3)_{i+1,j}}{(\bar{F}_1)_{i+1,j}} \tag{8.39}$$

$$(\bar{G}_2)_{i+1,j} = (\bar{F}_3)_{i+1,j} \tag{8.40}$$

$$(\bar{G}_3)_{i+1,j} = \bar{\rho}_{i+1,j}\left(\frac{\bar{F}_3}{\bar{F}_1}\right)^2_{i+1,j} + (\bar{F}_2)_{i+1,j} - \frac{(\bar{F}_1)^2_{i+1,j}}{\bar{\rho}_{i+1,j}} \tag{8.41}$$

$$(\bar{G}_4)_{i+1,j} = \frac{\gamma}{\gamma - 1}\left[(\bar{F}_2)_{i+1,j} - \frac{(\bar{F}_1)^2_{i+1,j}}{\bar{\rho}_{i+1,j}}\right]\left(\frac{\bar{F}_3}{\bar{F}_1}\right)_{i+1,j} + \frac{\bar{\rho}_{i+1,j}}{2}\left(\frac{\bar{F}_3}{\bar{F}_1}\right)_{i+1,j}\left[\left(\frac{\bar{F}_1}{\bar{\rho}}\right)^2_{i+1,j} + \left(\frac{\bar{F}_3}{\bar{F}_1}\right)^2_{i+1,j}\right] \tag{8.42}$$

Corrector step. On the corrector step, we return to Eqs. (8.30) to (8.33), with

rearward differences used for the η derivatives. Analogous to Eq. (6.29), we have

$$\left(\frac{\overline{\partial F_1}}{\partial \xi}\right)_{i+1,j} = \left(\frac{\partial \eta}{\partial x}\right)\frac{(\bar{F}_1)_{i+1,j-1} - (\bar{F}_1)_{i+1,j}}{\Delta \eta} + \frac{1}{h}\frac{(\bar{G}_1)_{i+1,j-1} - (\bar{G}_1)_{i+1,j}}{\Delta \eta} \tag{8.43a}$$

$$\left(\frac{\overline{\partial F_2}}{\partial \xi}\right)_{i+1,j} = \left(\frac{\partial \eta}{\partial x}\right)\frac{(\bar{F}_2)_{i+1,j-1} - (\bar{F}_2)_{i+1,j}}{\Delta \eta} + \frac{1}{h}\frac{(\bar{G}_2)_{i+1,j-1} - (\bar{G}_2)_{i+1,j}}{\Delta \eta} \tag{8.43b}$$

$$\left(\frac{\overline{\partial F_3}}{\partial \xi}\right)_{i+1,j} = \left(\frac{\partial \eta}{\partial x}\right)\frac{(\bar{F}_3)_{i+1,j-1} - (\bar{F}_3)_{i+1,j}}{\Delta \eta} + \frac{1}{h}\frac{(\bar{G}_3)_{i+1,j-1} - (\bar{G}_3)_{i+1,j}}{\Delta \eta} \tag{8.43c}$$

$$\left(\frac{\overline{\partial F_4}}{\partial \xi}\right)_{i+1,j} = \left(\frac{\partial \eta}{\partial x}\right)\frac{(\bar{F}_4)_{i+1,j-1} - (\bar{F}_4)_{i+1,j}}{\Delta \eta} + \frac{1}{h}\frac{(\bar{G}_4)_{i+1,j-1} - (\bar{G}_4)_{i+1,j}}{\Delta \eta} \tag{8.43d}$$

Forming the average derivatives analogous to Eq. (6.30), we have

$$\left(\frac{\partial F_1}{\partial \xi}\right)_{\text{av}} = \frac{1}{2}\left[\left(\frac{\partial F_1}{\partial \xi}\right)_{i,j} + \left(\frac{\overline{\partial F_1}}{\partial \xi}\right)_{i+1,j}\right] \tag{8.44a}$$

$$\left(\frac{\partial F_2}{\partial \xi}\right)_{\text{av}} = \frac{1}{2}\left[\left(\frac{\partial F_2}{\partial \xi}\right)_{i,j} + \left(\frac{\overline{\partial F_2}}{\partial \xi}\right)_{i+1,j}\right] \tag{8.44b}$$

$$\left(\frac{\partial F_3}{\partial \xi}\right)_{\text{av}} = \frac{1}{2}\left[\left(\frac{\partial F_3}{\partial \xi}\right)_{i,j} + \left(\frac{\overline{\partial F_3}}{\partial \xi}\right)_{i+1,j}\right] \tag{8.44c}$$

$$\left(\frac{\partial F_4}{\partial \xi}\right)_{\text{av}} = \frac{1}{2}\left[\left(\frac{\partial F_4}{\partial \xi}\right)_{i,j} + \left(\frac{\overline{\partial F_4}}{\partial \xi}\right)_{i+1,j}\right] \tag{8.44d}$$

where the derivatives on the right-hand side of Eqs. (8.44*a*) to (8.44*d*) are known numbers, known from Eqs. (8.36*a*) to (8.36*d*) and Eqs. (8.43*a*) to (8.43*d*). Finally,

analogous to Eq. (6.25), we have

$$(F_1)_{i+1,j} = (F_1)_{i,j} + \left(\frac{\partial F_1}{\partial \xi}\right)_{\text{av}} \Delta \xi \tag{8.45a}$$

$$(F_2)_{i+1,j} = (F_2)_{i,j} + \left(\frac{\partial F_2}{\partial \xi}\right)_{\text{av}} \Delta \xi \tag{8.45b}$$

$$(F_3)_{i+1,j} = (F_3)_{i,j} + \left(\frac{\partial F_3}{\partial \xi}\right)_{\text{av}} \Delta \xi \tag{8.45c}$$

$$(F_4)_{i+1,j} = (F_4)_{i,j} + \left(\frac{\partial F_4}{\partial \xi}\right)_{\text{av}} \Delta \xi \tag{8.45d}$$

Our calculation of the flow field (via the flux variables F_1 to F_4) at the next downstream location $i + 1$ is now complete, except for one remaining aspect—artificial viscosity. In the present problem, the sharp expansion corner located at $x = 10$ m (see Fig. 8.4) is a singular point; it introduces a discontinuous change in the surface flow properties at that point. The system of finite-difference equations developed above sees this discontinuity through a discontinuous change in the metric term $\partial\eta/\partial x$, which from Eqs. (8.25*a*) and (8.25*b*) is zero just ahead of the corner and $(1 - \eta)(\tan\theta)/h$ just behind the corner. Such a discontinuous change always has the potential to introduce oscillations in the numerical solution. Indeed, this author's experience in solving the present problem has shown that such oscillations do indeed develop in the flow field—oscillations which are virtually eliminated by including some artificial viscosity in the solution. The formulation of the artificial viscosity term for the present case follows the discussion given in Sec. 6.6 and is patterned after Eqs. (6.58) to (6.61). For the present case, we formulate the artificial viscosity term as follows. On the predictor step,

$$(SF_1)_{i,j} = \frac{C_y|p_{i,j+1} - 2p_{i,j} + p_{i,j-1}|}{p_{i,j+1} + 2p_{i,j} + p_{i,j-1}} \times [(F_1)_{i,j+1} - 2(F_1)_{i,j} + (F_1)_{i,j-1}] \tag{8.46a}$$

$$(SF_2)_{i,j} = \frac{C_y|p_{i,j+1} - 2p_{i,j} + p_{i,j-1}|}{p_{i,j+1} + 2p_{i,j} + p_{i,j-1}} \times [(F_2)_{i,j+1} - 2(F_2)_{i,j} + (F_2)_{i,j-1}] \tag{8.46b}$$

Similar expressions are obtained for $(SF_3)_{i,j}$ and $(SF_4)_{i,j}$; we do not need to take the space to write the corresponding equations. The values of $(SF_1)_{i,j}$, $(SF_2)_{i,j}$, etc., are added to Eqs. (8.37*a*) to (8.37*d*) as follows:

$$(\bar{F}_1)_{i+1,j} = (F_1)_{i,j} + \left(\frac{\partial F_1}{\partial \xi}\right)_{i,j} \Delta \xi + (SF_1)_{i,j} \tag{8.47a}$$

$$(\bar{F}_2)_{i+1,j} = (F_2)_{i,j} + \left(\frac{\partial F_2}{\partial \xi}\right)_{i,j} \Delta \xi + (SF_2)_{i,j} \tag{8.47b}$$

and similarly for $[\bar{F}_3]_{i+1,j}$ and $[\bar{F}_4]_{i+1,j}$. Artificial viscosity is also added on the corrector step as follows.

$$(\bar{S}\bar{F}_1)_{i+1,j} = \frac{C_y|\bar{p}_{i+1,j+1} - 2\bar{p}_{i+1,j} + \bar{p}_{i+1,j-1}|}{\bar{p}_{i+1,j+1} + 2\bar{p}_{i+1,j} + \bar{p}_{i+1,j-1}} \times [(\bar{F}_1)_{i+1,j+1} - 2(\bar{F}_1)_{i+1,j} + (\bar{F}_1)_{i+1,j-1}] \quad (8.48a)$$

$$(\bar{S}\bar{F}_2)_{i+1,j} = \frac{C_y|\bar{p}_{i+1,j+1} - 2\bar{p}_{i+1,j} + \bar{p}_{i+1,j-1}|}{\bar{p}_{i+1,j+1} + 2\bar{p}_{i+1,j} + \bar{p}_{i+1,j-1}} \times [(\bar{F}_2)_{i+1,j+1} - 2(\bar{F}_2)_{i+1,j} + (\bar{F}_2)_{i+1,j-1}] \quad (8.48b)$$

Similar expressions are obtained for $(\bar{S}\bar{F}_3)_{i+1,j}$ and $(\bar{S}\bar{F}_4)_{i+1,j}$. Finally, these values of artificial viscosity are added to Eqs. (8.45*a*) to (8.45*d*) as follows:

$$(F_1)_{i+1,j} = (F_1)_{i,j} + \left(\frac{\partial F_1}{\partial \xi}\right)_{\text{av}} \Delta\xi + (\bar{S}\bar{F}_1)_{i+1,j} \quad (8.49a)$$

$$(F_2)_{i+1,j} = (F_2)_{i,j} + \left(\frac{\partial F_2}{\partial \xi}\right)_{\text{av}} \Delta\xi + (\bar{S}\bar{F}_2)_{i+1,j} \quad (8.49b)$$

and similarly for $(F_3)_{i+1,j}$ and $(F_4)_{i+1,j}$. This completes the addition of artificial viscosity to the above algorithm.

Finally, the primitive variables at grid point $(i + 1, j)$ can be decoded from the values of $(F_1)_{i+1,j}$, $(F_2)_{i+1,j}$, $(F_3)_{i+1,j}$, and $(F_4)_{i+1,j}$ using Eqs. (8.8) to (8.12). This totally completes the calculation of the flow field at the next downstream location $i + 1$ at all the vertically arranged grid points in the internal part of the flow, from grid point $j = 2$ to $j = 40$. We have one remaining item to discuss, namely, the flow solution for the grid points at the boundaries, i.e., at $j = 1$ and 41.

BOUNDARY CONDITIONS. At the wall, the physically proper boundary condition for an inviscid flow is that the flow be tangent to the wall. This is the *only* boundary condition at the wall; all other flow properties at the wall must be obtained as part of the solution. As innocent as this may sound, in terms of the CFD calculation the proper numerical treatment of this wall boundary condition is not always straightforward; indeed, it has been the subject of much research in CFD. In the present case, we will employ a treatment of the wall boundary condition patterned after that suggested by Abbett (Ref. 46). For a steady flow, the steps in Abbett's boundary condition treatment are as follows.

1. Consider point 1 on the wall, as sketched in Fig. 8.5. Calculate trial values of u_1 and v_1 at point 1 using *one-sided differences* in the internal flow algorithm, i.e., using Eqs. (8.36*a*) to (8.49*b*), except modifying the corrector step to use forward differences just as on the predictor step. At the wall, this is the only choice, because we have no grid points below the wall and hence no way of forming the rearward differences called for on the corrector step. This use of forward-forward differences on the predictor-corrector sequence at the wall compromises slightly the second-order accuracy of the algorithm at the wall.

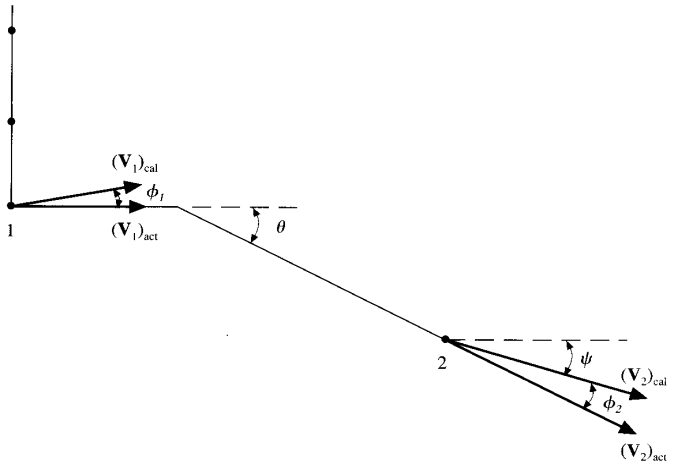

FIG. 8.5
Abbett's boundary condition for a steady flow.

2. The *direction* of the resultant velocity at the wall calculated in step 1 will not necessarily be tangent to the wall due to numerical inaccuracy. Usually, the calculated value of the velocity vector at the wall $(\mathbf{V}_1)_{\text{cal}}$ in Fig. 8.5, will make an angle ϕ_1 at the wall, where

$$\phi_1 = \tan^{-1}\frac{v_1}{u_1} \quad (8.50)$$

Also, the calculated Mach number at the wall will be

$$(M_1)_{\text{cal}} = \frac{\sqrt{(u_1)^2_{\text{cal}} + (v_1)^2_{\text{cal}}}}{(a_1)_{\text{cal}}} \quad (8.51)$$

Along with this value of $(M_1)_{\text{cal}}$ is a corresponding value of the Prandtl–Meyer function f_{cal}, obtained by substituting $(M_1)_{\text{cal}}$ into the right-hand side of Eq. (8.2).

3. Assume that the supersonic flow calculated at point 1 in step 2 is *rotated through a local centered Prandtl–Meyer expansion wave* so that the velocity vector is tangent to the wall. That is, $(\mathbf{V}_1)_{\text{cal}}$ in Fig. 8.5 is rotated through a Prandtl–Meyer expansion wave where the deflection angle through the wave is ϕ_1. This yields a new velocity vector $(\mathbf{V}_1)_{\text{act}}$, which is assumed to be the actual velocity tangent to the wall. The Mach number associated with $(\mathbf{V}_1)_{\text{act}}$ is $(M_1)_{\text{act}}$, obtained as follows. First, calculate f_{act} which corresponds to $(M_1)_{\text{act}}$ from the Prandtl–Meyer relationship given by Eq. (8.1), namely

$$f_{\text{act}} = f_{\text{cal}} + \phi_1 \quad (8.52)$$

In Eq. (8.52), f_{cal} is known from step 2, and ϕ_1 is the deflection angle shown in Fig. 8.5 and known from Eq. (8.50). The value of f_{act} calculated from Eq. (8.52) is that value corresponding to $(M_1)_{act}$, namely, the Mach number which exists *after* the flow is rotated to be parallel to the wall. The value of $(M_1)_{act}$ must be backed out of Eq. (8.2) by substituting f_{act} into the left-hand side and solving Eq. (8.2) by trial and error for $(M_1)_{cal}$.

4. Let the values of pressure, temperature, and density as originally calculated in step 1 (using one-sided differences) be denoted by p_{cal}, T_{cal}, and ρ_{cal}, respectively. These values must be changed to correspond to the new, "actual" conditions after the calculated velocity vector is rotated through the expansion wave to be parallel to the wall. These new values, denoted by p_{act}, T_{act}, and ρ_{act}, are obtained from Eqs. (8.3) to (8.5), respectively, using M_{cal} and M_{act} as follows:

$$p_{act} = p_{cal}\left\{\frac{1 + [(\gamma - 1)/2]M_{cal}^2}{1 + [(\gamma - 1)/2]M_{act}^2}\right\}^{\gamma/(\gamma-1)} \tag{8.53}$$

$$T_{act} = T_{cal}\frac{1 + [(\gamma - 1)/2]M_{cal}^2}{1 + [(\gamma - 1)/2]M_{act}^2} \tag{8.54}$$

$$\rho_{act} = \frac{p_{act}}{RT_{act}} \tag{8.55}$$

The values of p_{act}, T_{act}, and ρ_{act} calculated from Eqs. (8.53) to (8.55), respectively, are interpreted to be the final values of p, T, and ρ at grid point 1 at the wall.

Interpretation: What are we really doing by imposing the above boundary condition calculation? Returning to Fig. 8.5, we recall that the velocity at the wall as calculated from the internal flow algorithm using one-sided, forward differences on both the predictor and corrector steps will, in general, *not* be tangent to the wall. That is, there will be a *finite* normal component of velocity at the wall, v_1. The function of Abbett's boundary condition as described above is to simply *cancel* this calculated finite vertical velocity component by means of an imaginary, local, Prandtl–Meyer expansion wave at the wall. This local expansion wave is just an *artifice* which we use in the numerical calculation; it does not say that nature is actually doing this in the real flow. (Indeed, nature always does the right thing and never requires such an artifice.) However, consistent with this artifice of a local expansion wave, we must slightly modify the values of p, T, and ρ originally calculated at point 1 to be somewhat compatible with the cancellation of the finite v_1 at the wall by the expansion wave. Hence, at the flow boundary, namely, at point 1, when the calculation is finished, not only is the velocity now tangent to the wall but the pressure, temperature, and density at the wall are taken to be p_{act}, T_{act}, and ρ_{act} as calculated from Eqs. (8.53) to (8.55).

Note that, in the above procedure, if $(\mathbf{V}_1)_{cal}$ turns out to point *into* the wall, rather than out of the wall as sketched in Fig. 8.5, then a local Prandtl–Meyer isentropic *compression* wave is assumed. This implies only that ϕ_1 is now considered to be a *negative value* in Eq. (8.52); all other steps in the calculation remain the same.

For that portion of the wall behind the expansion corner, the above technique is still the same. Focusing on point 2 in Fig. 8.5, $(\mathbf{V}_2)_{cal}$ is rotated through the angle ϕ_2 to be tangent to the wall. Equation (8.52) now becomes

$$f_{act} = f_{cal} + \phi_2 \tag{8.56}$$

All aspects of the calculation at point 2 are carried out exactly as described above for point 1, with the exception that ϕ_2 is not given by Eq. (8.50). Instead, from the geometry shown at point 2 in Fig. 8.5, we have

$$\psi = \tan^{-1}\frac{|v_2|}{u_2} \tag{8.57}$$

and

$$\phi_2 = \theta - \psi \tag{8.58}$$

CALCULATION OF DOWNSTREAM MARCHING STEP SIZE. As discussed in Sec. 3.4.1, the governing flow equations for steady, inviscid, supersonic flow are hyperbolic; this is why a downstream-marching solution is well-posed. Moreover, in Sec. 4.5 we indicated that the proper stability criterion for linear hyperbolic equations is the CFL (Courant–Friedrichs–Lewy) criterion. An equation for the maximum allowable marching step according to the CFL criterion was developed in Sec. 4.5 for the case of time marching. We have stated that, on a physical basis, the maximum allowable time step for an explicit time-marching solution (based on the CFL criterion) should be less than, or at best equal to, the time required for a sound wave to move from one grid point to the next, adjacent grid point.

With this interpretation involving the propagation of sound waves, we can intuitively develop the CFL criterion for steady flow. Consider the sketch shown in Fig. 8.6, which shows a vertical array of grid points at a given x station. A small disturbance (e.g., a sound wave) introduced at point 1 will propagate along the two characteristic lines through point 1 (recall our discussion in the Steady, Inviscid Supersonic Flow subsection of Sec. 3.4.1); the characteristic lines are Mach lines in the flow, which are at the Mach angle μ relative to the streamline direction. If the angle made by the streamline at point 1 is θ relative to the x axis, then the angles made by the left- and right-running Mach waves relative to the x axis are $\theta + \mu$ and $\theta - \mu$, respectively. In Fig. 8.6, only the left-running Mach line is shown at point 1. Consider a horizontal line through point 2; the left-running characteristic from point 1 intersects this horizontal line at point a. Point a is therefore located a distance $(\Delta x)_1$ from point 2, where

$$\Delta x_1 = \frac{\Delta y}{\tan(\theta + \mu)_1} \tag{8.59}$$

Based on the CFL criterion applied locally at point 2, the downstream value chosen for Δx should be no more than $(\Delta x)_1$ for stability; in this fashion the distance between points 2 and a is less than, or at most equal to, the distance required for a sound wave from point 1 to reach the level defined by the y location of point 2. A

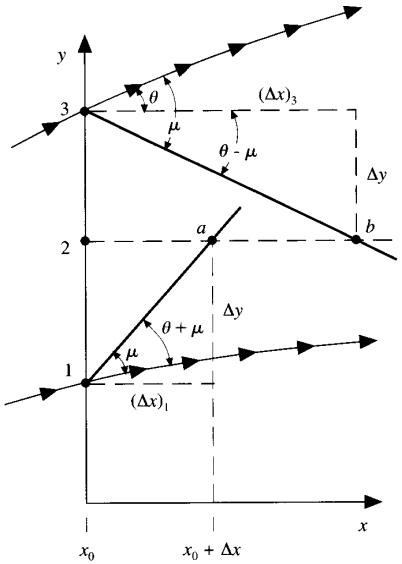

FIG. 8.6
Sketch in the physical plane for the calculation of the marching step size.

similar argument regarding the right-running Mach wave through point 3 shows that it intersects the horizontal line through point 2 at point b. Point b is therefore located a distance $(\Delta x)_3$ from point 2, where

$$(\Delta x)_3 = \frac{\Delta y}{\tan(\theta - \mu)_3} \tag{8.60}$$

For stability of the downstream marching calculations locally at point 2, the chosen value of the step size Δx should be no more than the minimum of $(\Delta x)_1$ and $(\Delta x)_3$. Expanding this argument to *all* the grid points arrayed along the vertical line at x_0, we can express the value of Δx to be chosen for the next downstream marching step at x_0 to be given by

$$\Delta x = \frac{\Delta y}{|\tan(\theta \pm \mu)|_{\max}} \tag{8.61}$$

where $|\tan(\theta + \mu)|_{\max}$ is the *maximum* of the absolute values of $\tan(\theta \pm \mu)$ evaluated for *all* the grid points arrayed along the vertical line at $x = x_0$. Since the transformation defined by Eqs. (8.19) and (8.20) states that $\xi = x$, then the proper step size for downstream marching in the computational plane shown in Fig. 8.3*b* is

$$\Delta\xi \leq \Delta x \tag{8.62}$$

where Δx is given by Eq. (8.61). Combining Eq. (8.62) with Eq. (8.61) and introducing the Courant number C, we have as our stability criterion for the value of $\Delta\xi$,

$$\boxed{\Delta\xi = C\frac{\Delta y}{|\tan(\theta \pm \mu)|_{\max}}} \tag{8.63}$$

where the CFL criterion states that $C \leq 1$. The value of $\Delta\xi$ obtained from Eq. (8.63) is the value that goes into Eqs. (8.37*a*) to (8.37*d*) and Eqs. (8.45*a*) to (8.45*d*).

8.3.3 Intermediate Results

Once again, we will follow our philosophy of giving some intermediate results during the course of a calculation so that you can check some intermediate numbers from your own computer program; if you are not writing your own program for this application, the present section still provides educational value for you—it is essentially a glorified flow diagram for the numerical solution.

Starting from the initial conditions given in Table 8.1 at $x = 0$ and using a Courant number $C = 0.5$ in Eq. (8.63), we find that after taking 16 marching steps downstream, we are located at $x = 12.928$ m. Examining Fig. 8.4, this station is located 2.928 m downstream of the expansion corner. Let us focus on the calculations associated with the second grid point at this station, i.e., the grid point labeled $j = 2$ in Fig. 8.7, which shows the local grid in the vicinity of the wall in the region around $\xi = 12.928$ m. In the finite-difference procedure, the station $\xi = 12.928$ m represents the location at which the flow is to be calculated from the known values at the previous station. Hence, $\xi = 12.928$ m corresponds to location $i + 1$ in the finite-difference equations given in Sec. 8.3.2, and the previous station corresponds to location i.

Using the stability criterion given by Eq. (8.63), with $C = 0.5$, the value of $\Delta\xi$ between stations i and $i + 1$ in Fig. 8.7 is $\Delta\xi = 0.818$ m. Hence, at station i, $\xi = 12.928 - 0.818 = 12.11$ m. At this station i, we have from Eq. (8.35),

$$h = 40 + (12.11 - 10)\tan 5.352^\circ = 40.20 \text{ m}$$

Also, the metric $\partial\eta/\partial x$ evaluated at grid point $j = 2$ at station i is, from Eq. (8.25*b*),

$$\frac{\partial\eta}{\partial x} = (1 - \eta)\frac{\tan\theta}{h} = (1 - 0.025)\frac{\tan 5.352}{40.20} = 2.272 \times 10^{-3} \text{ m}^{-1}$$

At station i, the values of F_1 at points $j = 1$, 2, and 3 are known from the calculations at the previous step. These values are $(F_1)_{i,1} = 0.696 \times 10^3 \frac{kg}{m^2 \cdot s}$,

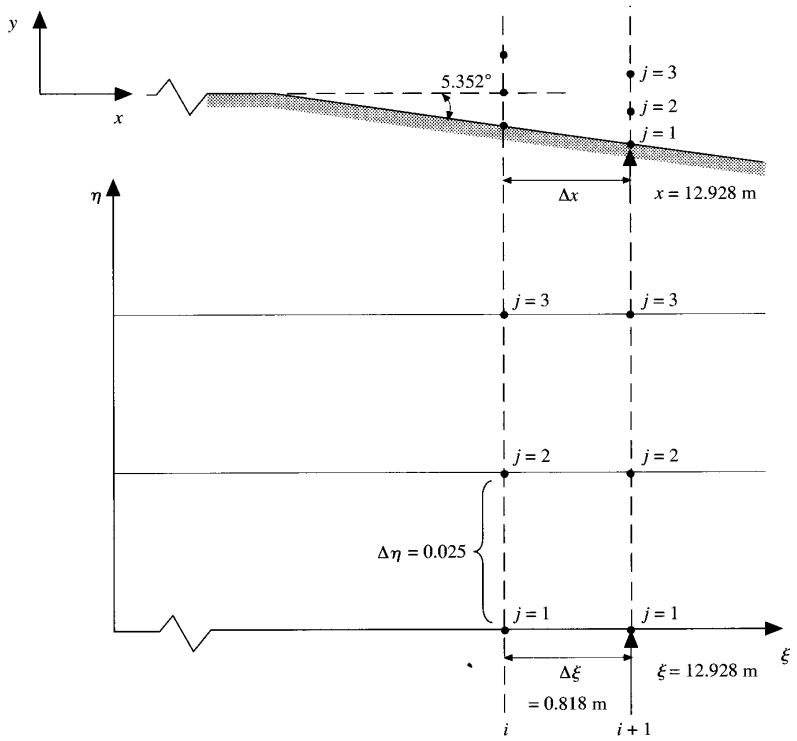

FIG. 8.7
Local grid adjacent to the wall at station $x = \xi = 12.928$ m.

$(F_1)_{i,2} = 0.744 \times 10^3 \frac{kg}{(m^2 \cdot s)}$, and $(F_1)_{i,3} = 0.798 \times 10^3 \frac{kg}{(m^2 \cdot s)}$. From eq. (8.36a), we have

$$\left(\frac{\partial F_1}{\partial \xi}\right)_{i,2} = \left(\frac{\partial \eta}{\partial x}\right)_{i,2} \frac{(F_1)_{i,2} - (F_1)_{i,3}}{\Delta \eta} + \frac{1}{h_i} \frac{(G_1)_{i,2} - (G_1)_{i,3}}{\Delta \eta}$$

$$= (2.272 \times 10^{-3}) \left[\frac{(0.744 - 0.798) \times 10^3}{0.025}\right] + \frac{1}{40.20} \left[\frac{(-0.435 + 0.193) \times 10^3}{0.025}\right]$$

$$= -4.908 - 24.080 = \boxed{-28.99 \text{ kg/(m}^3 \cdot \text{s)}}$$

From Eq. (8.37*a*), we have

$$(\bar{F}_1)_{i+1,2} = (F_1)_{i,2} + \left(\frac{\partial F_1}{\partial \xi}\right)_{i,2} \Delta \xi$$

$$= 0.744 \times 10^3 + (-28.99)(0.818)$$

$$= 0.720 \times 10^3 \text{ kg/(m}^2 \cdot \text{s)}$$

At this stage, we add some artificial viscosity. From Eq. (8.46*a*) we have, where $C_y = 0.6$,

$$(SF_1)_{i+1,2} = \frac{C_y |p_{i+1,3} - 2p_{i+1,2} + p_{i+1,1}|}{p_{i+1,3} + 2p_{i+1,2} + p_{i+1,1}} \times [(F_1)_{i+1,3} - 2(F_1)_{i+1,2} + (F_1)_{i+1,1}]$$

$$= 0.001 \times 10^3$$

From Eq. (8.47*a*), we have

$$(\bar{F}_1)_{i+1,2} = (F_1)_{i,2} + \left(\frac{\partial F}{\partial \xi}\right)_{i,2} \Delta \xi + (SF_1)_{i+1,2}$$

$$= 0.720 \times 10^3 + 0.001 \times 10^3$$

$$= \boxed{0.721 \times 10^3 \text{ kg/(m}^2 \cdot \text{s)}}$$

Note how small is the value of the artificial viscosity compared to the magnitude of the variable to which it is being added. This is as it should be, since the calculations are being made in a region where only small gradients of the flow-field variables exist, and hence artificial viscosity is not a strong player here. From the same calculations applied at grid points $(i, 1)$ and $(i, 3)$, we have

$$(\bar{F}_1)_{i+1,1} = 0.703 \times 10^3 \text{ kg/(m}^2 \cdot \text{s)}$$

$$(\bar{F}_1)_{i+1,3} = 0.783 \times 10^3 \text{ kg/(m}^2 \cdot \text{s)}$$

Also, from the sequential application of Eqs. (8.36*b*) to (8.36*d*) and Eqs. (8.37*b*) to (8.37*d*) we find that

$$(\bar{F}_2)_{i+1,2} = 0.585 \times 10^6 \text{ N/m}^2$$

$$(\bar{F}_3)_{i+1,2} = -0.388 \times 10^5 \text{ kg/(m} \cdot \text{s}^2)$$

$$(\bar{F}_4)_{i+1,2} = 0.372 \times 10^9 \text{ N/(m} \cdot \text{s)}$$

The predicted density at point $(i + 1, 2)$ is obtained from Eq. (8.38), where

$$A = \frac{(\bar{F}_3)^2_{i+1,2}}{2(\bar{F}_1)_{i+1,2}} - (\bar{F}_4)_{i+1,2}$$

$$= \frac{(-0.388 \times 10^5)^2}{2(0.721 \times 10^3)} - 0.372 \times 10^9$$

$$= -0.37095 \times 10^9 \frac{\text{N}}{\text{m} \cdot \text{s}}$$

$$B = \frac{\gamma}{\gamma - 1}(\bar{F}_1)_{i+1,2}(\bar{F}_2)_{i+1,2}$$

$$= \frac{1.4}{0.4}(0.721 \times 10^3)(0.585 \times 10^6)$$

$$= 1.476 \times 10^9 \frac{\text{N}^2 \cdot \text{s}}{\text{m}^5}$$

$$C = -\frac{\gamma + 1(\bar{F}_1)^3_{i+1,j}}{2(\gamma - 1)}$$

$$= -\frac{2.4}{2(0.4)}(0.721 \times 10^3)^3 = 1.124 \times 10^9 \frac{\text{kg}}{\text{m}^2 \cdot \text{s}}$$

and

$$\bar{\rho}_{i+1,2} = \frac{-B + \sqrt{B^2 - 4AC}}{2A}$$

$$= \frac{-1.476 \times 10^9 + \sqrt{(1.476 \times 10^9)^2 - 4(0.372 \times 10^9)(1.124 \times 10^9)}}{2(-0.37095 \times 10^9)}$$

$$= \boxed{1.02 \text{ kg/m}^3}$$

With this, we can form the predicted values for G, for example, from Eq. (8.39):

$$(\bar{G}_1)_{i+1,2} = \bar{\rho}_{i+1,2}\frac{(\bar{F}_3)_{i+1,2}}{(\bar{F}_1)_{i+1,2}} = 1.02\left(\frac{-0.388 \times 10^5}{0.721 \times 10^3}\right)$$

$$= \boxed{-0.552 \times 10^2 \text{ kg/(m}^2 \cdot \text{s)}}$$

In a similar manner, we find that $[\bar{G}_1]_{i+1,1} = -0.658 \times 10^2$ kg/(m$^2 \cdot$ s).

With the above information, we move to the corrector step. From Eq. (8.43*a*),

$$\left(\frac{\partial \bar{F}_1}{\partial \xi}\right)_{i+1,2} = \left(\frac{\partial \eta}{\partial x}\right)\frac{(\bar{F}_1)_{i+1,1} - (\bar{F})_{i+1,2}}{\Delta \eta} + \frac{1}{h}\frac{(\bar{G}_1)_{i+1,1} - (\bar{G}_1)_{i+1,2}}{\Delta \eta}$$

At this stage we have a choice to make; in the above equation, do we evaluate $\partial \eta/\partial x$ and h at station i or $i + 1$? It is not immediately obvious which choice to make. It

appears that we are evaluating the left-hand side of the equation at station $i + 1$. On the other hand, this equation is simply one element of a calculation that seeks to represent an *average* value of the flow-field derivatives between locations i and $i + 1$, and hence it might be appropriate to treat $\partial \eta/\partial x$ and h consistently as those values at station i on *both* the predictor and corrector step. Faced with this choice, we make the latter. Hence, in the above equation we will use the value of the metric and the value of h as those existing at station i. With this, we obtain

$$\left(\frac{\partial \bar{F}_1}{\partial \xi}\right)_{i+1,2} = (2.272 \times 10^{-3})\left[\frac{(0.703 - 0.721) \times 10^3}{0.025}\right]$$

$$+ \frac{1}{40.2}\left[\frac{(-0.658 + 0.552) \times 10^2}{0.025}\right]$$

$$= \boxed{-0.122 \times 10^2 \text{ kg/(m}^3 \cdot \text{s)}}$$

From Eq. (8.44*a*), we have

$$\left(\frac{\partial F_1}{\partial \xi}\right)_{\text{av}} = \frac{1}{2}\left[\left(\frac{\partial F_1}{\partial \xi}\right)_{i,2} + \left(\frac{\overline{\partial F}}{\partial \xi}\right)_{i+1,2}\right]$$

$$= \tfrac{1}{2}(-28.99 - 12.2) = \boxed{-20.5 \text{ kg/(m}^3 \cdot \text{s)}}$$

From Eq. (8.45*a*)

$$(F_1)_{i+1,2} = (F_1)_{i,2} + \left(\frac{\partial F}{\partial \xi}\right)_{\text{av}} \Delta \xi$$

$$= 0.744 \times 10^3 + (-20.5)(0.818)$$

$$= 0.727 \times 10^3 \text{ kg/(m}^2 \cdot \text{s)}$$

At this stage, we add some artificial viscosity. From Eq. (8.48*a*), we find that

$$(\bar{S}\bar{F}_1)_{i+1,2} = -0.8$$

Hence, from Eq. (8.49*a*)

$$(F_1)_{i+1,2} = (F_1)_{i,2} + \left(\frac{\partial F_1}{\partial \xi}\right)_{\text{av}} \Delta \xi + (\bar{S}\bar{F}_1)_{i+1.2}$$

$$= \boxed{0.728 \times 10^3 \text{ kg/(m}^2 \cdot \text{s)}}$$

In a similar manner, we obtain

$$(F_2)_{i+1.2} = 0.590 \times 10^6 \frac{\text{N}}{\text{m}^2}$$

$$(F_3)_{i+1.2} = -0.36 \times 10^5 \frac{\text{kg}}{\text{m} \cdot \text{s}^2}$$

$$(F_4)_{i+1,2} = 0.375 \times 10^9 \frac{\text{N}}{\text{m} \cdot \text{s}}$$

Decoding the primitive variables as described earlier, we have from Eq. (8.8)

$$A = \frac{(F_3)^2_{i+1,2}}{2(F_1)^2_{i+1,2}} - (F_4)_{i+1,2}$$

$$= \frac{(-0.36 \times 10^5)^2}{2(0.728 \times 10^3)} - 0.375 \times 10^9$$

$$= -0.374 \times 10^9 \frac{\text{N}}{\text{m} \cdot \text{s}}$$

$$B = \frac{\gamma}{\gamma - 1}(F_1)_{i+1,2}(F_2)_{i+1,2}$$

$$= \left(\frac{1.4}{0.4}\right)(0.728 \times 10^3)(0.590 \times 10^6) = 1.503 \times 10^9 \frac{\text{N} \cdot \text{s}}{\text{m}^5}$$

$$C = \frac{-(\gamma + 1)}{2(\gamma - 1)}(F_1)^3_{i+1,2}$$

$$= \frac{-(2.4)}{0.8}(0.728 \times 10^3)^3 = 1.152 \times 10^9 \left(\frac{\text{kg}}{\text{m}^2 \cdot \text{s}}\right)^3$$

Thus,

$$\rho_{i+1,2} = \frac{-B + \sqrt{B^2 - 4AC}}{2A}$$

$$= \frac{-1.503 \times 10^9 + \sqrt{(-1.50 \times 10^9)^2 - 4(-0.374 \times 10^9)(1.152 \times 10^9)}}{2(-0.374 \times 10^9)}$$

$$= \boxed{1.04 \text{ kg/m}^3}$$

From Eq. (8.9)

$$u_{i+1,2} = \frac{(F_1)_{i+1,2}}{\rho_{i+1,2}} = \frac{0.728 \times 10^3}{1.04} = \boxed{701 \text{ m/s}}$$

From Eq. (8.10)

$$v_{i+1,2} = \frac{(F_3)_{i+1,2}}{(F_1)_{i+1,2}} = \frac{-0.36 \times 10^5}{0.728 \times 10^3} = \boxed{-49.4 \text{ m/s}}$$

From Eq. (8.11)

$$p_{i+1,2} = (F_2)_{i+1,2} - (F_1)_{i+1,2}u_{i+1,2}$$

$$= 0.590 \times 10^6 - (0.728 \times 10^3)(701)$$

$$= \boxed{0.795 \times 10^5 \text{ N/m}^2}$$

Finally, from Eq. (8.11) we have

$$T_{i+1,2} = \frac{p_{i+1,2}}{R\rho_{i+1,2}} = \frac{0.795 \times 10^5}{287(1.04)} = \boxed{267 \text{ K}}$$

Return to Fig. 8.7. In the above calculations, we have illustrated how the flow-field values at grid point $j = 2$ located at station $i + 1$ are computed from the known flow field at station i. Let us now concentrate on the calculation of the flow field at the boundary, i.e., at grid point $j = 1$ at station $i + 1$ in Fig. 8.7. To avoid repetitiveness, we will examine the calculation on the corrector step; the treatment of the boundary condition on the predictor step follows the same approach.

We first need to calculate the values of F_1, F_2, etc., at the boundary using one-sided, forward differences on both the predictor and corrector steps. We will pick up the calculation on the corrector step. From Eq. (8.43*a*), but with forward differences, we have

$$\left(\frac{\overline{\partial F_1}}{\partial \xi}\right)_{i+1,1} = \left(\frac{\partial \eta}{\partial x}\right)\frac{(\bar{F}_1)_{i+1,1} - (\bar{F}_1)_{i+1,2}}{\Delta \eta} + \frac{1}{h}\frac{(\bar{G}_1)_{i+1,1} - (\bar{G}_1)_{i+1.2}}{\Delta \eta}$$

From the predictor step, we have values for the quantities on the right-hand side of the above equations; they are

$$(\bar{F}_1)_{i+1,1} = 0.703 \times 10^3 \frac{\text{kg}}{\text{m}^2 \cdot \text{s}} \qquad (\bar{F}_1)_{i+1,2} = 0.721 \times 10^3 \frac{\text{kg}}{\text{m}^2 \cdot \text{s}}$$

$$(\bar{G}_1)_{i+1,1} = -0.658 \times 10^2 \frac{\text{kg}}{\text{m}^2 \cdot \text{s}} \qquad (\bar{G}_1)_{i+1,2} = -0.552 \times 10^2 \frac{\text{kg}}{\text{m}^2 \cdot \text{s}}$$

Thus,

$$\left(\frac{\overline{\partial F_1}}{\partial \xi}\right)_{i+1,1} = (2.272 \times 10^{-3})\left[\frac{(0.703 - 0.721) \times 10^3}{0.025}\right]$$

$$+ \frac{1}{40.20}\left[\frac{(-0.658 + 0.552) \times 10^2}{0.025}\right]$$

$$= -1.64 - 10.55 = -12.18 \text{ kg/(m}^3 \cdot \text{s)}$$

Also from the predictor step, we have

$$\left(\frac{\partial F}{\partial \xi}\right)_{i,1} = -26.1 \text{ kg/(m}^3 \cdot \text{s)}$$

From Eq. (8.44*a*),

$$\left(\frac{\partial F}{\partial \xi}\right)_{\text{av}} = \frac{1}{2}\left[\left(\frac{\partial F_1}{\partial \xi}\right)_{i,1} + \left(\frac{\overline{\partial F}}{\partial \xi}\right)_{i+1,1}\right]$$

$$= \tfrac{1}{2}[(-26.1) + (-12.18)] = -19.14 \text{ kg/(m}^3 \cdot \text{s)}$$

From Eq. (8.45*a*)

$$(F_1)_{i+1,1} = (F_1)_{i,1} + \left(\frac{\partial F}{\partial \xi}\right)_{\text{av}} \Delta\xi$$
$$= 0.696 \times 10^3 + (-19.14)(0.818)$$
$$= 0.680 \times 10^3 \text{ kg/(m}^2 \cdot \text{s)}$$

This is the value of F_1 at the boundary as obtained from the algorithm designed for the *internal* flow-field points, modified for one-sided differences at the wall. Analogous results are obtained for F_2, F_3, and F_4 at the boundary. These values are then decoded to obtain the primitive variables at the wall. The results are

$$M_{\text{cal}} = 2.22$$
$$p_{\text{cal}} = 0.705 \times 10^5 \text{ N/m}^2$$
$$T_{\text{cal}} = 255 \text{ K}$$
$$\rho_{\text{cal}} = 0.963 \text{ kg/m}^3$$
$$v_{\text{cal}} = -74.6 \text{ m/s}$$
$$u_{\text{cal}} = 707 \text{ m/s}$$

Note that the calculated values of v_{cal} and u_{cal} yield a velocity vector in the direction defined by the angle ψ in Fig. 8.5. From Eq. (8.57),

$$\psi = \tan^{-1}\frac{|v_{\text{cal}}|}{u_{\text{cal}}} = \tan^{-1}\frac{74.6}{707} = 6.02°$$

However, the wall downstream of the expansion corner is at an angle $\theta = 5.353°$ (see Fig. 8.5). Thus, after the use of the one-sided differences at the wall as described above, we see that the calculated velocity vector is pointing *into* the wall, since $\psi > \theta$ (again, see Fig. 8.5). From Eq. (8.58), we have

$$\phi_2 = \theta - \psi = 5.352 - 6.02 = -0.668°$$

Hence, we need to *imagine* that the *calculated* supersonic flow at the wall must be rotated through an angle $\phi_2 = -0.668°$ (an upward rotation) in order to be tangent to the wall; this rotation is carried out by means of a local Prandtl–Meyer *compression* wave, since the calculated flow is *into* the wall. From Eq. (8.56)

$$f_{\text{act}} = f_{\text{cal}} + \phi_2$$

Since $f_{\text{cal}} = 32.24°$ for $M_{\text{cal}} = 2.22$, we have

$$f_{\text{act}} = 32.24 - 0.668 = 31.57°$$

From Eq. (8.2), this yields

$$M_{\text{act}} = 2.19$$

The actual values of pressure, temperature, and density at the wall are obtained from Eqs. (8.53) to (8.55), respectively.

$$p_{i+1,1} = p_{\text{act}} = p_{\text{cal}}\left\{\frac{1 + [(\gamma-1)/2]M_{\text{cal}}^2}{1 + [(\gamma-1)/2]M_{\text{act}}^2}\right\}^{\gamma/(\gamma-1)}$$
$$= (0.705 \times 10^5)\left[\frac{1 + 0.4(2.22)^2}{1 + 0.4(2.19)^2}\right]^{3.5}$$
$$= \boxed{0.734 \times 10^5 \text{ N/m}^2}$$
$$T_{i+1,1} = T_{\text{act}} = T_{\text{cal}}\frac{1 + [(\gamma-1)/2]M_{\text{cal}}^2}{1 + [(\gamma-1)/2]M_{\text{act}}^2}$$
$$= 255\left[\frac{1 + 0.4(2.22)^2}{1 + 0.4(2.19)^2}\right] = \boxed{258 \text{ K}}$$
$$\rho_{i+1,1} = \rho_{\text{act}} = \frac{p_{\text{act}}}{RT_{\text{act}}} = \frac{0.734 \times 10^5}{287(258)} = \boxed{0.992 \text{ kg/m}^3}$$

The use of the local Prandtl–Meyer wave at the wall to rotate the calculated velocity vector so that it becomes tangent to the wall is purely a conceptual matter; it is simply a way to *imagine* that the component of the calculated velocity *perpendicular* to the wall, which is usually a finite value when the one-sided differences are used, is *canceled* by means of the local Prandtl–Meyer wave. (Keep in mind that the proper flow tangency boundary condition can be expressed by stating that the component of velocity normal to the wall must be *zero*.) The actual values of p, T, and ρ obtained above represent a small *adjustment* to the originally calculated values to be consistent with this cancellation of the normal velocity component.

Finally, since the local Prandtl–Meyer wave is functioning to simply cancel the normal component of velocity, and this cancellation involves only a small velocity change, we choose to leave the x-component velocity, as calculated from one-sided differences, alone. That is, we will stipulate that

$$u_{i+1,1} = u_{\text{cal}} = 707 \text{ m/s}$$

From this, the corresponding y component of velocity at the wall must be the following value, after the normal component is effectively canceled and the flow is therefore tangent to the wall.

$$v_{i+1,1} = -u_{i+1,1}\tan\theta = -707\tan 5.352° = \boxed{-66.2 \text{ m/s}}$$

Note that this value of v is slightly smaller than $v_{\text{cal}} = -74.6$ m/s as listed above, calculated from one-sided differences. The value $v_{i+1,1} = -66.2$ m/s is compatible with the flow tangency boundary condition.

This ends our sample, intermediate calculations. For completeness, the results obtained at all the grid points from $j = 1$ to $j = 41$ at the station located at

$x = \xi = 12.928$ m are tabulated in Tables 8.2 and 8.3. The numbers tabulated here are the final flow-field values obtained from the downstream-marching technique at the station $x = 12.928$ m; this corresponds to the sixteenth marching step starting from the given initial conditions at $x = 0$. We will return to Tables 8.2 and 8.3 during our final analysis of the results as discussed in the next section.

TABLE 8.2
Results at $x = 12.928$ m

j	y, m	η	u, m/s	v, m/s	ρ, kg/m^3	p, N/m^3
1	−0.274	0.000	.707E+03	−.662E+02	.992E+00	.734E+05
2	0.733	0.025	.701E+03	−.494E+02	.104E+01	.795E+05
3	1.739	0.050	.691E+03	−.266E+02	.112E+01	.891E+05
4	2.746	0.075	.683E+03	−.869E+01	.119E+01	.969E+05
5	3.753	0.100	.679E+03	−.131E+01	.122E+01	.100E+06
6	4.760	0.125	.678E+03	−.148E−01	.123E+01	.101E+06
7	5.767	0.150	.678E+03	.326E−05	.123E+01	.101E+06
8	6.774	0.175	.678E+03	−.167E−03	.123E+01	.101E+06
9	7.781	0.200	.678E+03	.472E−04	.123E+01	.101E+06
10	8.787	0.225	.678E+03	−.702E−04	.123E+01	.101E+06
11	9.794	0.250	.678E+03	−.195E−04	.123E+01	.101E+06
12	10.801	0.275	.678E+03	.180E−04	.123E+01	.101E+06
13	11.808	0.300	.678E+03	−.598E−04	.123E+01	.101E+06
14	12.815	0.325	.678E+03	−.642E−04	.123E+01	.101E+06
15	13.822	0.350	.678E+03	−.325E−13	.123E+01	.101E+06
16	14.829	0.375	.678E+03	.000E+00	.123E+01	.101E+06
17	15.835	0.400	.678E+03	.000E+00	.123E+01	.101E+06
18	16.842	0.425	.678E+03	.000E+00	.123E+01	.101E+06
19	17.849	0.450	.678E+03	.000E+00	.123E+01	.101E+06
20	18.856	0.475	.678E+03	.000E+00	.123E+01	.101E+06
21	19.863	0.500	.678E+03	.000E+00	.123E+01	.101E+06
22	20.870	0.525	.678E+03	.000E+00	.123E+01	.101E+06
23	21.877	0.550	.678E+03	.000E+00	.123E+01	.101E+06
24	22.883	0.575	.678E+03	.000E+00	.123E+01	.101E+06
25	23.890	0.600	.678E+03	.217E−10	.123E+01	.101E+06
26	24.897	0.625	.678E+03	.118E−03	.123E+01	.101E+06
27	25.904	0.650	.678E+03	.120E−03	.123E+01	.101E+06
28	26.911	0.675	.678E+03	.354E−05	.123E+01	.101E+06
29	27.918	0.700	.678E+03	.125E−03	.123E+01	.101E+06
30	28.925	0.725	.678E+03	−.193E−04	.123E+01	.101E+06
31	29.931	0.750	.678E+03	−.607E−04	.123E+01	.101E+06
32	30.938	0.775	.678E+03	.242E−03	.123E+01	.101E+06
33	31.945	0.800	.678E+03	.160E−03	.123E+01	.101E+06
34	32.952	0.825	.678E+03	.161E−03	.123E+01	.101E+06
35	33.959	0.850	.678E+03	.401E−04	.123E+01	.101E+06
36	34.966	0.875	.678E+03	−.848E−04	.123E+01	.101E+06
37	35.973	0.900	.678E+03	−.128E−03	.123E+01	.101E+06
38	36.979	0.925	.678E+03	−.342E−04	.123E+01	.101E+06
39	37.986	0.950	.678E+03	−.107E−03	.123E+01	.101E+06
40	38.993	0.975	.678E+03	−.636E−04	.123E+01	.101E+06
41	40.000	1.000	.678E+03	.000E+00	.123E+01	.101E+06

TABLE 8.3
Flux values at $x = 12.928$ m

j	T, K	M	F_1, kg/(m^2 · s)	F_2, N/m^2	F_3, kg/(m · s^2)	F_4, N/(m · s)
1	.258E+03	.220E+01	.701E+03	.569E+06	−.464E+05	.358E+09
2	.267E+03	.215E+01	.728E+03	.590E+06	−.360E+05	.375E+09
3	.277E+03	.208E+01	.776E+03	.626E+06	−.207E+05	.402E+09
4	.283E+03	.203E+01	.815E+03	.654E+06	−.708E+04	.422E+09
5	.286E+03	.200E+01	.831E+03	.665E+06	−.109E+04	.430E+09
6	.286E+03	.200E+01	.834E+03	.667E+06	−.123E+02	.431E+09
7	.286E+03	.200E+01	.834E+03	.667E+06	.272E−02	.431E+09
8	.286E+03	.200E+01	.834E+03	.667E+06	−.140E+00	.431E+09
9	.286E+03	.200E+01	.834E+03	.667E+06	.394E−01	.431E+09
10	.286E+03	.200E+01	.834E+03	.667E+06	−.586E−01	.431E+09
11	.286E+03	.200E+01	.834E+03	.667E+06	−.162E−01	.431E+09
12	.286E+03	.200E+01	.834E+03	.667E+06	.150E−01	.431E+09
13	.286E+03	.200E+01	.834E+03	.667E+06	−.499E−01	.431E+09
14	.286E+03	.200E+01	.834E+03	.667E+06	−.535E−01	.431E+09
15	.286E+03	.200E+01	.834E+03	.667E+06	−.271E−10	.431E+09
16	.286E+03	.200E+01	.834E+03	.667E+06	.000E+00	.431E+09
17	.286E+03	.200E+01	.834E+03	.667E+06	.000E+00	.431E+09
18	.286E+03	.200E+01	.834E+03	.667E+06	.000E+00	.431E+09
19	.286E+03	.200E+01	.834E+03	.667E+06	.000E+00	.431E+09
20	.286E+03	.200E+01	.834E+03	.667E+06	.000E+00	.431E+09
21	.286E+03	.200E+01	.834E+03	.667E+06	.000E+00	.431E+09
22	.286E+03	.200E+01	.834E+03	.667E+06	.000E+00	.431E+09
23	.286E+03	.200E+01	.834E+03	.667E+06	.000E+00	.431E+09
24	.286E+03	.200E+01	.834E+03	.667E+06	.000E+00	.431E+09
25	.286E+03	.200E+01	.834E+03	.667E+06	.181E−07	.431E+09
26	.286E+03	.200E+01	.834E+03	.667E+06	.988E−01	.431E+09
27	.286E+03	.200E+01	.834E+03	.667E+06	.100E+00	.431E+09
28	.286E+03	.200E+01	.834E+03	.667E+06	.295E−02	.431E+09
29	.286E+03	.200E+01	.834E+03	.667E+06	.104E+00	.431E+09
30	.286E+03	.200E+01	.834E+03	.667E+06	−.161E−01	.431E+09
31	.286E+03	.200E+01	.834E+03	.667E+06	−.506E−01	.431E+09
32	.286E+03	.200E+01	.834E+03	.667E+06	.201E+00	.431E+09
33	.286E+03	.200E+01	.834E+03	.667E+06	.133E+00	.431E+09
34	.286E+03	.200E+01	.834E+03	.667E+06	.134E+00	.431E+09
35	.286E+03	.200E+01	.834E+03	.667E+06	.335E−01	.431E+09
36	.286E+03	.200E+01	.834E+03	.667E+06	−.707E−01	.431E+09
37	.286E+03	.200E+01	.834E+03	.667E+06	−.106E+00	.431E+09
38	.286E+03	.200E+01	.834E+03	.667E+06	−.285E−01	.431E+09
39	.286E+03	.200E+01	.834E+03	.667E+06	−.891E−01	.431E+09
40	.286E+03	.200E+01	.834E+03	.667E+06	−.530E−01	.431E+09
41	.286E+03	.200E+01	.834E+03	.667E+06	.000E+00	.431E+09

8.3.4 Final Results

Let us examine the results of the present downstream marching calculations in a more global fashion. Such a global picture is shown in Fig. 8.8. Here the x component of the velocity, u, is plotted versus the vertical distance y at five different stations in the x direction, namely, $x = 0$, 16.17, 32.31, 48.99, and 66.23 m. The

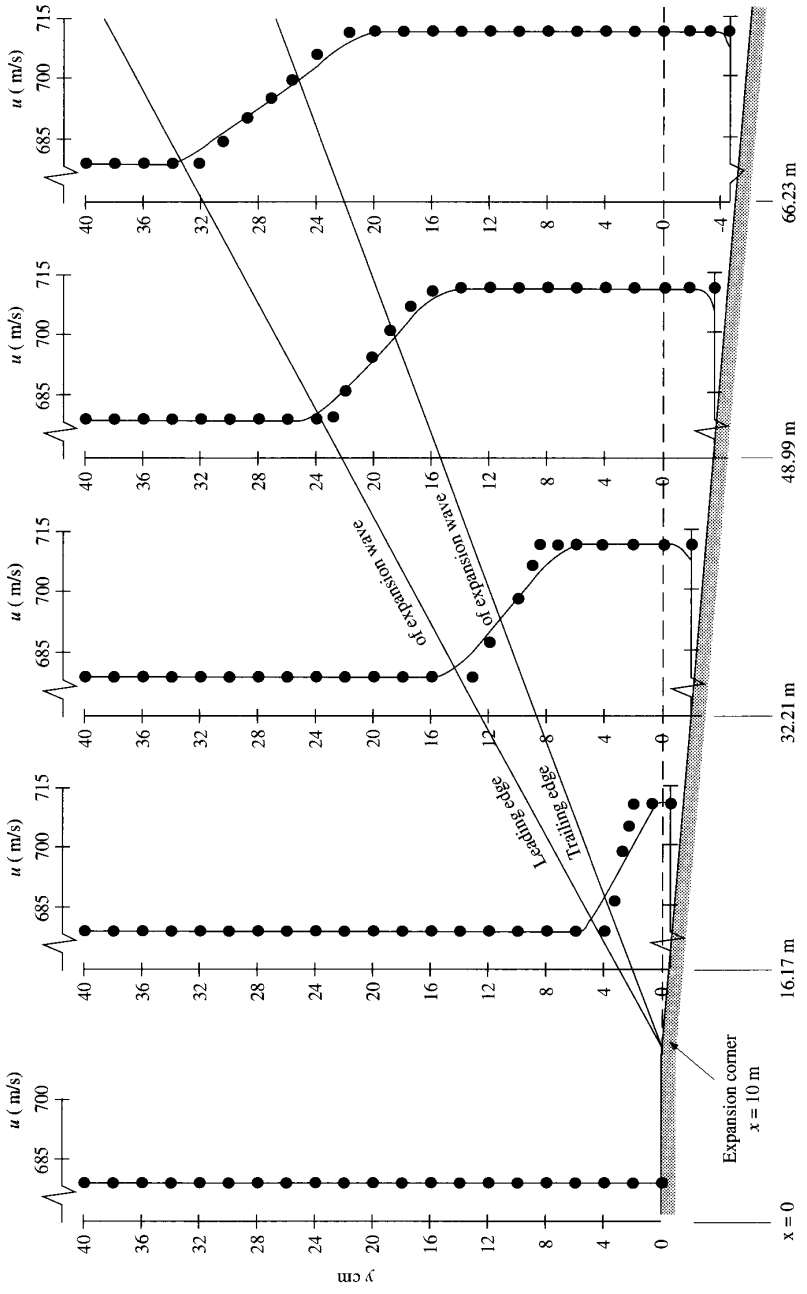

FIG. 8.8
Comparison between the CFD results and the exact, analytical solution (dark circles) for supersonic flow through a centered expansion wave. Solid lines are numerical results.

geometry of the wall, with the expansion corner at $x = 10$ m, is also plotted to scale. Moreover, the leading and trailing edges of the centered expansion wave (exact solution) are drawn to scale and superimposed on the figure. For each of the five velocity profiles shown, a comparison between the exact analytical results (the dark circles) and the numerical downstream marching, finite-difference results (the solid line) is given. Make certain to orient yourself with regard to what is shown in Fig. 8.8 before progressing further.

In Fig. 8.8, the velocity profile at $x = 0$ shows the uniform inflow conditions where $u = 678$ m/s. The velocity profile at $x = 16.17$ m is just slightly downstream of the expansion corner, which is located at $x = 10$ m. The station at $x = 16.17$ m corresponds to 20 marching steps downstream of the inlet. It is intuitively obvious that the most severe demands on the numerical solution are in the vicinity of the expansion corner, which analytically is a singular point. Reflecting back to the governing flow equations expressed by Eqs. (8.30) to (8.33), note that the metric $\partial\eta/\partial x$ experiences a discontinuous change at the expansion corner, as is clearly seen in Eqs. (8.25*a*) and (8.25*b*). Also, just behind the expansion corner, there are only a few vertically arrayed grid points between the wall and the trailing edge of the wave, and fewer points yet inside the wave itself. As a result, not only is the numerical solution in this region effectively hit over the head with a sledgehammer (i.e., in the form of the singular point and the discontinuity in the metric), there are also very few grid points available in that region to absorb the blow. The net result is the partial lack of definition of the wave at the $x = 16.17$ m station; the agreement between the numerical calculation and the exact, analytical results inside and behind the wave is not very good. This behavior is one of the reasons why a relatively mild expansion corner with a deflection angle of 5.352° is chosen for the present test case. For a larger deflection angle, the problems discussed above are exacerbated. Consider the case for a corner deflection angle of 23.38° with the same Mach 2 upstream flow in the present example. This flow deflection will expand the flow to Mach 3 downstream of the corner. However, when $\theta = 23.38°$ is fed into the current setup, the calculations develop some strong oscillations and eventually (about 6 or 8 m downstream of the corner) blow up. Presumably there is some combination of number of grid points with an appropriately heavy numerical damping (via large artificial viscosity) that might result in a successful solution downstream of the expansion corner for this large deflection case. This matter is left for you to examine.

At this stage, we recall that Tables 8.2 and 8.3 give the flow-field variables even closer to the expansion corner, namely, at $x = 12.928$ m. The numbers tabulated in those tables simply reinforce the above discussion.

As the numerical solution progressively marches further downstream, where the expansion wave is wider and the distance between the wall and the trailing edge of the wave is larger, the agreement between the exact, analytical results and the numerical computations improves considerably. Concentrating on the velocity profile at the $x = 66.23$ m station, we see good agreement; the numerical solution is capturing the wave in the right location, the variation of the computed velocity inside the wave nicely follows the exact, analytical solution, and the velocity downstream of the wave is uniform at the correct value.

There is a slightly disturbing phenomenon occurring right at the wall as the numerical calculations progress downstream. The exact, analytical value for u_2 downstream of the wave is 710.2 m/s. At $x = 16.17$ m, the numerical value of u_2 right at the wall is 711 m/s—very close to the exact result. However, as we march downstream, the value of u_2 at the wall begins to deviate; at the subsequent three downstream stations ($x = 32.3$, 48.99, and 66.23 m), the respective values of u_2 at the wall are 708, 707, and 705 m/s. This can be seen in Fig. 8.8 as a small "velocity layer" right at the wall, which departs from the exact solution. The thickness of this layer is only one grid increment, i.e., the thickness is only Δy. At the first grid point above the wall, the flow velocity comes into very good agreement with exact results. This small velocity layer, which is certainly a numerically induced phenomenon and *not* a physical result, may be due to the history of the expansion corner singularity being propagated downstream by the numerical computations. It also may be due to a progressive accumulation of numerical error owing to the numerical implementation of the boundary condition. Since the solution uses a downstream marching philosophy, numerical errors that occur upstream are simply carried along as the solution marches downstream. If a certain type of numerical error, no matter how slight, is repeatedly generated at the wall, it will have a tendency to accumulate as we march downstream. Perhaps a slight improvement in our numerical implementation of the flow tangency boundary condition is in order. This would be an interesting matter for you to examine.

Note from Fig. 8.8 that the leading edge of the exact expansion wave exits the computational domain through the *downstream* boundary, i.e., at about a height $y = 32.5$ m. The geometry of our computational space is chosen intentionally to allow this to happen. Recall that the boundary condition we are imposing at the *upper* boundary (at $\eta = 1.0$) is simply the specification of uniform conditions equal to those in the uniform flow upstream of the expansion wave. This is appropriate as long as the expansion wave completely exits the computational space along the vertical, downstream boundary at $x = 66.23$ m. Imagine what would happen if we were to continue marching downstream, say to a station $x = 100$ m. By examining Fig. 8.8, we can easily see that the leading edge and part of the internal portion of the expansion wave will exit through the upper boundary. If and when such a situation exits, we must use a different boundary condition along the upper boundary—different from that which we have used so far. In this case, what changes would you make along the upper boundary? A simple thought is the calculation of the flow properties along the upper boundary from the flow equations using one-sided differences (in this case requiring one-sided rearward differences on both the predictor and corrector steps). Another possibility is to extrapolate the values to the upper boundary from information at the internal grid points; however, in this case, rather than using a linear extrapolation in the vertical direction, it would be more appropriate to extrapolate along *characteristic lines* from the internal grid points. This is something else with which you might want to experiment.

Return to the results shown in Fig. 8.8. For the sake of completeness, all the computed flow-field variables at the $x = 66.23$ station (which corresponds to 80 marching steps from the inlet) are tabulated in Tables 8.4 and 8.5. When examining these tabulated results, it is useful to note that the exact, analytical values

TABLE 8.4
Results at $x = 66.278$ m

j	y, m	η	u, m/s	v, m/s	ρ, kg/m^3	p, N/m^3
1	−5.272	0.000	.705E+03	−.661E+02	.109E+01	.731E+05
2	−4.140	0.025	.710E+03	−.682E+02	.107E+01	.730E+05
3	−3.009	0.050	.711E+03	−.690E+02	.969E+00	.732E+05
4	−1.877	0.075	.711E+03	−.688E+02	.977E+00	.731E+05
5	−0.745	0.100	.711E+03	−.689E+02	.976E+00	.731E+05
6	0.387	0.125	.711E+03	−.688E+02	.976E+00	.731E+05
7	1.519	0.150	.711E+03	−.689E+02	.976E+00	.731E+05
8	2.650	0.175	.711E+03	−.690E+02	.976E+00	.731E+05
9	3.782	0.200	.711E+03	−.690E+02	.976E+00	.731E+05
10	4.914	0.225	.711E+03	−.688E+02	.977E+00	.731E+05
11	6.046	0.250	.711E+03	−.686E+02	.977E+00	.732E+05
12	7.178	0.275	.711E+03	−.688E+02	.977E+00	.731E+05
13	8.309	0.300	.711E+03	−.694E+02	.975E+00	.729E+05
14	9.441	0.325	.711E+03	−.696E+02	.974E+00	.729E+05
15	10.573	0.350	.711E+03	−.690E+02	.976E+00	.731E+05
16	11.705	0.375	.711E+03	−.678E+02	.980E+00	.735E+05
17	12.837	0.400	.711E+03	−.672E+02	.982E+00	.737E+05
18	13.968	0.425	.711E+03	−.683E+02	.978E+00	.733E+05
19	15.100	0.450	.712E+03	−.708E+02	.970E+00	.725E+05
20	16.232	0.475	.713E+03	−.732E+02	.963E+00	.717E+05
21	17.364	0.500	.713E+03	−.740E+02	.960E+00	.714E+05
22	18.496	0.525	.713E+03	−.726E+02	.964E+00	.719E+05
23	19.627	0.550	.711E+03	−.693E+02	.975E+00	.730E+05
24	20.759	0.575	.709E+03	−.647E+02	.990E+00	.746E+05
25	21.891	0.600	.707E+03	−.591E+02	.101E+01	.765E+05
26	23.023	0.625	.705E+03	−.531E+02	.103E+01	.787E+05
27	24.155	0.650	.702E+03	−.468E+02	.105E+01	.810E+05
28	25.287	0.675	.699E+03	−.405E+02	.107E+01	.834E+05
29	26.418	0.700	.696E+03	−.343E+02	.110E+01	.859E+05
30	27.550	0.725	.693E+03	−.283E+02	.112E+01	.883E+05
31	28.682	0.750	.690E+03	−.227E+02	.114E+01	.907E+05
32	29.814	0.775	.688E+03	−.175E+02	.116E+01	.930E+05
33	30.946	0.800	.685E+03	−.129E+02	.118E+01	.950E+05
34	32.077	0.825	.683E+03	−.901E+01	.119E+01	.968E+05
35	33.209	0.850	.681E+03	−.591E+01	.121E+01	.982E+05
36	34.341	0.875	.680E+03	−.361E+01	.121E+01	.993E+05
37	35.473	0.900	.679E+03	−.203E+01	.122E+01	.100E+06
38	36.605	0.925	.679E+03	−.105E+01	.123E+01	.100E+06
39	37.736	0.950	.678E+03	−.499E+00	.123E+01	.101E+06
40	38.868	0.975	.678E+03	−.229E+00	.123E+01	.101E+06
41	40.000	1.000	.678E+03	.000E+00	.123E+01	.101E+06

TABLE 8.5
Flux values at $x = 66.278$ m

j	T, K	M	F_1, kg/(m^2 · s)	F_2, N/m^2	F_3, kg/(m · s^2)	F_4, N/(m · s)
1	.233E+03	.231E+01	.769E+03	.616E+06	−.508E+05	.374E+09
2	.237E+03	.231E+01	.760E+03	.612E+06	−.519E+05	.374E+09
3	.263E+03	.220E+01	.689E+03	.563E+06	−.475E+05	.358E+09
4	.261E+03	.221E+01	.694E+03	.567E+06	−.478E+05	.359E+09
5	.261E+03	.221E+01	.694E+03	.567E+06	−.478E+05	.359E+09
6	.261E+03	.221E+01	.694E+03	.567E+06	−.478E+05	.359E+09
7	.261E+03	.221E+01	.694E+03	.567E+06	−.478E+05	.359E+09
8	.261E+03	.221E+01	.694E+03	.567E+06	−.479E+05	.359E+09
9	.261E+03	.221E+01	.694E+03	.567E+06	−.479E+05	.359E+09
10	.261E+03	.221E+01	.694E+03	.567E+06	−.478E+05	.359E+09
11	.261E+03	.221E+01	.695E+03	.567E+06	−.477E+05	.359E+09
12	.261E+03	.221E+01	.695E+03	.567E+06	−.478E+05	.359E+09
13	.261E+03	.221E+01	.693E+03	.566E+06	−.481E+05	.359E+09
14	.261E+03	.221E+01	.693E+03	.566E+06	−.483E+05	.358E+09
15	.261E+03	.221E+01	.694E+03	.567E+06	−.479E+05	.359E+09
16	.261E+03	.220E+01	.697E+03	.569E+06	−.472E+05	.360E+09
17	.261E+03	.220E+01	.698E+03	.569E+06	−.469E+05	.361E+09
18	.261E+03	.221E+01	.696E+03	.568E+06	−.475E+05	.360E+09
19	.260E+03	.221E+01	.691E+03	.564E+06	−.489E+05	.357E+09
20	.259E+03	.222E+01	.686E+03	.561E+06	−.502E+05	.355E+09
21	.259E+03	.222E+01	.685E+03	.560E+06	−.506E+05	.354E+09
22	.260E+03	.222E+01	.687E+03	.562E+06	−.499E+05	.356E+09
23	.261E+03	.221E+01	.694E+03	.566E+06	−.481E+05	.359E+09
24	.262E+03	.219E+01	.703E+03	.573E+06	−.454E+05	.363E+09
25	.264E+03	.218E+01	.713E+03	.581E+06	−.422E+05	.369E+09
26	.266E+03	.216E+01	.725E+03	.590E+06	−.385E+05	.375E+09
27	.269E+03	.214E+01	.737E+03	.599E+06	−.345E+05	.382E+09
28	.271E+03	.212E+01	.750E+03	.608E+06	−.304E+05	.388E+09
29	.273E+03	.210E+01	.763E+03	.617E+06	−.262E+05	.394E+09
30	.275E+03	.209E+01	.775E+03	.625E+06	−.220E+05	.401E+09
31	.277E+03	.207E+01	.786E+03	.634E+06	−.178E+05	.407E+09
32	.279E+03	.205E+01	.797E+03	.641E+06	−.139E+05	.412E+09
33	.281E+03	.204E+01	.807E+03	.648E+06	−.104E+05	.417E+09
34	.283E+03	.203E+01	.815E+03	.654E+06	−.734E+04	.422E+09
35	.284E+03	.202E+01	.822E+03	.658E+06	−.485E+04	.425E+09
36	.285E+03	.201E+01	.826E+03	.661E+06	−.298E+04	.428E+09
37	.285E+03	.201E+01	.830E+03	.664E+06	−.169E+04	.429E+09
38	.286E+03	.200E+01	.832E+03	.665E+06	−.877E+03	.430E+09
39	.286E+03	.200E+01	.833E+03	.666E+06	−.416E+03	.431E+09
40	.286E+03	.200E+01	.834E+03	.666E+06	−.191E+03	.431E+09
41	.286E+03	.200E+01	.834E+03	.667E+06	.000E+00	.431E+09

downstream of the expansion wave are

$$M_2 = 2.20$$
$$p_2 = 0.739 \times 10^5 \text{ N/m}^2$$
$$\rho_2 = 0.984 \text{ kg/m}^3$$
$$T_2 = 262 \text{ K}$$
$$u_2 = 710 \text{ m/s}$$
$$v_2 = -66.5 \text{ m/s}$$

In Tables 8.4 and 8.5, if we compare the numerical results in the uniform region downstream of the wave (say between $j = 2$ and 23) with the exact analytical results listed above, we find the following percentage errors.

Quantity	% error
M_2	0.45
p_2	1.08
ρ_2	0.813
T_2	0.038
u_2	0.141
v_2	3.76

This agreement between the exact analytical solution for the flow behind an expansion wave and the corresponding numerical results is reasonable; indeed, the percentage errors listed above are on par with those obtained in Chap. 7 for our time-marching solutions of nozzle flows. The only disturbing feature shown in Tables 8.4 and 8.5 are the values at the wall ($j = 0$). Here we see the presence of some type of "error layer" at the wall, as discussed earlier in regard to the velocity profiles in Fig. 8.8. The velocity is not the only variable affected by this phenomena; the other flow variables exhibit a slight change at the wall compared to the values immediately above it (except for the pressure, which is virtually constant in the region of the wall, including the wall point.) Our earlier discussion on this matter is sufficient; we will not repeat it here. Suffice it to say that such behavior is an example that *CFD is not perfect*—a fact which is important for you to appreciate.

In regard to the matter of grid independence, a solution was carried out where the number of grid points in the y direction was doubled; i.e., the value of Δy (hence $\Delta\eta$) was halved. This led to 81 points being distributed in the y direction. Also, since the marching step $\Delta\xi$ is related to $\Delta\eta$ through the stability criterion (see Eq. 8.63), this also doubled the number of grid points in the ξ direction. The net result was an increase in the number of grid points by a factor of 4. The calculated results for the flow field in this case were not materially different from those discussed earlier. Therefore, the earlier results basically reflect grid independence.

As a final comment in this section, note that the geometric units chosen to describe the *size* of the computational space for the above calculations, namely, a height of about 40 m and a length of about 65 m, is irrelevant to the answer. Instead

of using meters, we could just as well as chosen millimeters, with a computational space of 40 mm by 65 mm, or any other length units for that matter. The flow problem of the supersonic flow through an expansion wave does not depend on any particular length scale. Since in the present calculations we chose to solve the governing equations in *dimensional* variables, we had to stipulate some geometric length; to maintain *consistent* units, we chose the unit of meters. So if a length of 65 m sounds very large to you, do not worry; it is totally irrelevant to the solution of the problem.

8.4 SUMMARY

The major items discussed and illustrated in this chapter are diagrammed in the road map shown in Fig. 8.9. The main thrust of this chapter is to highlight the philosophy of space marching in contrast to that of time marching discussed in Chap. 7. Such space marching required us to use the conservation form of the steady flow equations. The geometry of the problem requires a boundary-fitted coordinate system, so this gave us a chance to work with some aspects of grid generation and to use the governing equations in the transformed space. Moreover, we used the technique of wave capturing, albeit here we captured an expansion wave rather than a shock wave as done in Chap. 7; with wave capturing, we already appreciate the need to use the conservation form of the governing equations. We also applied some artificial viscosity to smooth the results; this is mainly needed in the vicinity of the expansion corner, which itself is a mathematical singularity. For the rest of the expansion wave, we most likely could do without the artificial viscosity. Finally, for the inviscid flow at the boundary, we utilized Abbett's numerical treatment of the boundary condition, which involved the use of a local, imaginary, Prandtl–Meyer wave at the wall to rotate the calculated velocity vector to be parallel to the wall. All

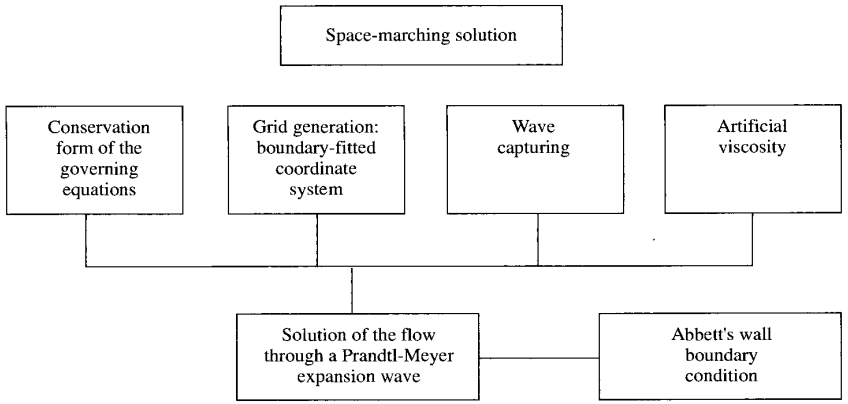

FIG. 8.9
Road map for Chap. 8.

these elements went into the calculation of the supersonic flow through a centered, Prandtl–Meyer expansion wave, which was the featured flow problem in this chapter.

At this stage, we are reminded that the CFD techniques used in both Chaps. 7 and 8 are *explicit* finite-difference techniques. To expand our horizons, it is time for us to explore an *implicit* solution applied to an appropriate flow problem. This leads us directly to the next chapter.